Quaternary Science Reviews 317 (2023) 108274

Contents lists available at ScienceDirect

Quaternary Science Reviews

journal homepage: www.elsevier.com/locate/quascirev

Early Holocene thinning and final demise of the Scandinavian Ice Sheet across the main drainage divide of southern Norway

Anders Romundset [a,*], Naki Akçar [b], Ola Fredin [d], Jane L. Andersen [c], Fredrik Høgaas [a], Marcus Christl [e], Serdar Yesilyurt [f], Christian Schlüchter [b]

[a] NGU, Geological Survey of Norway, Trondheim, Norway
[b] Institute of Geological Sciences, University of Bern, Bern, Switzerland
[c] Department of Geoscience, Aarhus University, Denmark
[d] Department of Geoscience and Petroleum, Norwegian University of Science and Technology (NTNU), Norway
[e] Laboratory of Ion Beam Physics, ETH Zurich, Switzerland
[f] Ankara University, Department of Geography, Ankara, Turkey

ARTICLE INFO

Handling Editor: C. O'Cofaigh

Keywords:
Ice sheet thinning
Scandinavian Ice Sheet
Gudbrandsdalen
Ice-dammed lake
Surface exposure dating

ABSTRACT

The thinning and final decay of the Scandinavian Ice Sheet in the Gudbrandsdalen area in central southern Norway is described, based on (1) cosmogenic ^{10}Be surface exposure dating of 25 glacially transported boulders, (2) radiocarbon dating of plant remains in the basal strata in four lakes and (3) mapping of large ice-dammed lakes that formed at different elevations and at different times during the last deglacation. We complement the new chronology with previously published ^{10}Be-ages from the same region. The dated samples are spread from mountain summits 1800 m a.s.l. to the valley floor at 250 m a.s.l. Our results suggest that the ice sheet surface remained well above 1800 m a.s.l. in northern Gudbrandsdalen throughout the Younger Dryas. During the Early Holocene the ice sheet thinned rapidly, at rates estimated to 1.7–5.8 m yr^{-1}. The final phase of deglaciation involved formation of large ice-dammed lakes, most notably the Store Dølasjø which was formed after 10.4 ka BP and finally drained around 10.0 ka BP. The ice-marginal landforms that characterize the mountain region of northern Gudbrandsdalen, i.e., moraine ridges, lateral meltwater channels, as well as deposits and shorelines from ice-dammed lakes, thus collectively originate from a period of rapid ice sheet downwasting over ca. 1600 years.

1. Introduction

The northern part of the deep, glacially incised Gudbrandsdalen valley in southern Norway is surrounded by ~2000 m high mountains (Fig. 1). This landscape provides a rich geomorphological legacy of the vertically downwasting ice sheet during the last deglaciation (Hansen, 1890; Rekstad, 1896; Holmsen, 1918b; Mannerfelt, 1945, 1949; Gjessing, 1960). Most importantly, widespread series of lateral meltwater channels are found along the mountain sides, and the bottom of the main valley is characterized by glaciolacustrine deposits and shorelines from a major ice-dammed lake (IDL), named the Store Dølasjø IDL by Garnes and Bergersen (1980). The overall pattern of deglaciation in the Gudbrandsdalen area has been known for more than a century, but the timing has been almost unknown. Both regional and ice-sheet-wide reconstructions have been hampered by the poor chronology from this region (Nesje and Dahl, 1990; Mangerud et al., 2011; Hughes et al., 2016). Most reconstructions show gradual thinning of a dome-shaped ice sheet across southern Norway throughout the Late Glacial, but a contrasting view with extensive ice free mountains in central southern Norway prior to the Younger Dryas, has also been proposed (Dahl et al., 1997; Linge et al., 2006; Paus et al., 2011, 2015; Marr et al., 2019; Lane et al., 2020). This dissension concerns large ice volumes for eustatic sea-level budgets and Earth system models covering the last deglaciation (Peltier et al., 2015).

Moreover, the thinning rates and ice volume reduction of present-day ice sheets are key unknowns in predictive models for ice sheet

* Corresponding author. Geological Survey of Norway, Leiv Eirikssons veg 39, N-7040, Trondheim, Norway.
E-mail addresses: anders.romundset@ngu.no (A. Romundset), akcar@geo.unibe.ch (N. Akçar), ola.fredin@ntnu.no (O. Fredin), jane.lund@geo.au.dk (J.L. Andersen), fredrik.hogaas@ngu.no (F. Høgaas), mchristl@phys.ethz.ch (M. Christl), yesilyurt@ankara.edu.tr (S. Yesilyurt), christian.schluechter@geo.unibe.ch (C. Schlüchter).

https://doi.org/10.1016/j.quascirev.2023.108274
Received 7 June 2023; Received in revised form 8 August 2023; Accepted 14 August 2023
Available online 26 August 2023

Fig. 1. Map of southern Norway, showing the Younger Dryas ice margin and ice divide (Mangerud et al., 2023a), and marine shoreline isobases (Sørensen et al., 1987). Also shown is the Nedre Glomsjø ice-dammed lake (Høgaas and Longva, 2018), and the mapped extent and shoreline isobases for the Store Dølasjø ice-dammed lake (this work). For closer comparison of isobase directions (coastal vs. Store Dølasjø IDL), see Fig. 9.

behaviour and rising eustatic sea levels in a warming climate (Noble et al., 2020; Pörtner et al., 2022). Given the brief time interval covered by the instrumental record (i.e., satellite altimetry), palaeo-analogues are needed to get a firm understanding of how quickly ice sheets respond to external forcing (e.g., Small et al., 2019). The last deglaciation of the former Scandinavian Ice Sheet provides such an analogue, when the ice surface lowered, leading to waning and eventually stagnating ice flow (Patton et al., 2017).

In this paper we present a new deglaciation chronology from the northern Gudbrandsdalen area, based on the results from several complementary methods. We combine new and previously published ^{10}Be-ages from moraine ridges, erratic boulders and the bedrock surface, to establish the timing and rate of regional ice-sheet thinning. We have also mapped four large ice-dammed lakes (IDLs) that formed at different elevations during ice-sheet thinning. By comparing the tilt of the mapped shorelines with the regional crustal uplift pattern we obtain ages for the IDLs, thereby adding an independent chronology for the ice sheet thinning. The latest part of the deglaciation chronology is further constrained by radiocarbon-dated lake sediments that provide minimum ages for local deglaciation. The combination of different chronological datasets allows us to assess the validity of the ^{10}Be-based chronology and to identify outlier ages, resulting from inherited nuclides from previous exposure. Our study and results highlight the advantage of applying a range of methods to scrutinize the chronology of ice sheet thinning and regional development, during deglaciation across a diverse landscape.

2. Study area

The study area covers the northern part of the large Gudbrandsdalen valley, its neighbouring tributary valleys, and adjacent mountains in southern Norway (Fig. 2). The valley floor of Gudbrandsdalen rises from ca. 250 m a.s.l. near Vinstra (lower right corner in Fig. 2), to ca. 610 m a.s.l. at the main drainage divide between eastern and western Norway, at Lesjaskog in the northwest. Most of the valley floor is covered with alluvial and glaciolacustrine deposits, whereas valley sides and surrounding mountains are mostly barren or till-covered and heavily imprinted by deglacial meltwater erosion and post-glacial mass wasting (NGU, 2023). Extensive blockfields indicate limited glacial erosion above ca. 1500 m a.s.l. (Nesje et al., 1988; Bonow et al., 2003; Andersen et al., 2018). Still, erratic boulders occur also on the highest summits near 2000 m a.s.l. and document complete, probably cold-based ice cover during full glaciation (Stroeven et al., 2016). In some deeply incised side valleys, stratigraphical fabric analysis of thick till sequences have been used to reconstruct dominating ice flow directions through the Weichselian (Mangerud, 1965; Garnes and Bergersen, 1980). Initial ice build-up is assumed to have taken place in the mountains near the main drainage divide, with later southward migration of the ice divide. However, several localities with interstadial glaciofluvial deposits, some holding mammoth tusks and teeth, also document prolonged intervening ice-free periods in much of the area during the last glaciation (Heintz, 1955; Bergersen and Garnes, 1971; Heintz, 1974; Bergersen and Garnes, 1981; Hole and Bergersen, 1981; Mangerud et al., 2023b). Mapping of streamlined bedforms and glacial striae suggests that the ice sheet divide prior to the last deglaciation was located somewhat north of Vinstra, 50–100 km southeast of the main drainage divide (Mangerud et al., 2011). During ice-sheet thinning, surface melt across the ice sheet caused the formation of lateral meltwater channels along the mountain sides; their dip directions represent the ice surface gradient and indicate that the ice divide later during the deglaciation migrated farther south, near Vinstra (Fig. 1; Mangerud, 1963). The position of northern Gudbrandsdalen south of the main drainage divide, but north of the Late Weichselian ice divide (Fig. 1), is decisive for the course of the deglaciation in this area.

During ice sheet thinning, the ice remained longest near the former ice divide, and lakes were therefore ponded between the downwasting ice sheet and the drainage divide. Shoreline features marking the extent of former ice-dammed lakes (IDLs) can be traced along many valley and mountain sides (Sollid and Kristiansen, 1984; Sollid and Trollvik, 1991; NGU, 2023). Deglacial IDL shorelines are typically represented by laterally extensive, wave-cut abrasion scarps in till, beach ridges, perched terraces and deltas (e.g., Høgaas and Longva, 2018; Regnéll et al., 2019). The IDL shorelines can often be directly connected to local drainage divides that acted as spillways and are therefore characterized by distinct glaciofluvial landforms, owing to the large discharge of glacial meltwater. Glaciolacustrine lake-floor deposits (predominantly silt) cover extensive areas and can locally be tens of meters thick (Hansen, 1886; Holtedahl, 1960). Ever since the dawn of agriculture in northern Gudbrandsdalen, such lake deposits from the large Store Dølasjø IDL have been important for farming and land use. The Store Dølasjø shorelines were first recognised by the scientific community in the mid-1800s (Chambers, 1851) and, following much debate (Hansen, 1886, 1890; Reusch, 1894, 1910; Rekstad, 1896; Øyen, 1896), interpreted to have formed in an IDL, restricted by a glacier tongue occupying the Rosten valley narrowing (Fig. 2; Holmsen, 1918a). Later Garnes and Bergersen (1980) mapped and correlated shoreline features over a larger region, leading to the conclusion that the lake was much larger than originally believed and that the ice dam was located farther south, north of Vinstra (Fig. 2). They also discussed the Store Dølasjø IDL in context of the regional Weichselian glaciation history and concluded that it existed

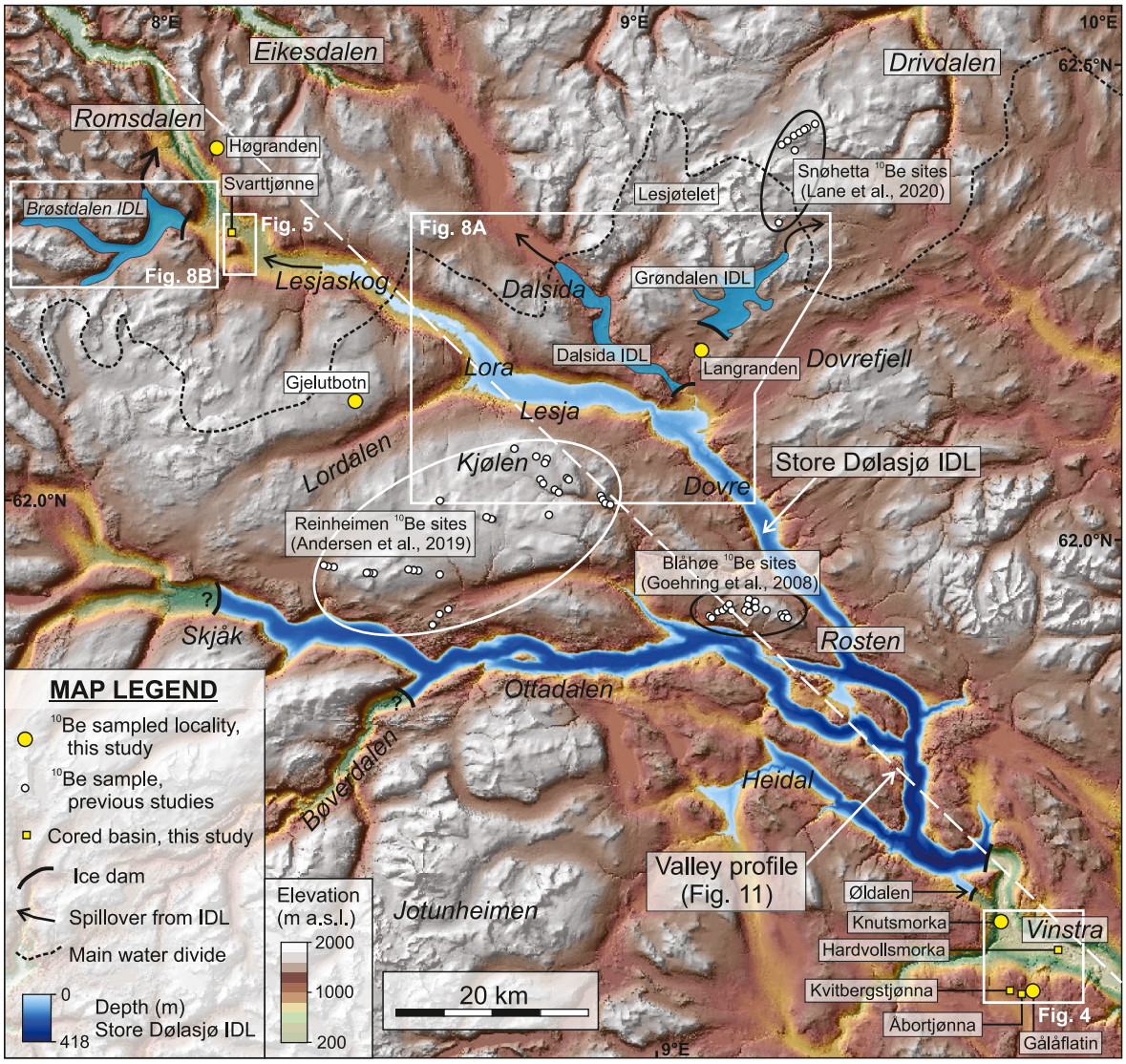

Fig. 2. Map of the northern Gudbrandsdalen region (box in Fig.1), showing the sample sites in this study, as well as reconstructed ice-dammed lakes. Also shown are sites from previous studies using ^{10}Be-dating in Reinheimen (Andersen et al., 2018), at Blåhøe (Goehring et al., 2008) and near Snøhetta (Lane et al., 2020). The stippled line marks the valley profile used in Fig. 11.

during the final phase of deglaciation.

3. Material and methods

3.1. 10Be surface exposure dating

To constrain ice-sheet thinning by cosmogenic surface exposure dating, we sampled boulders found at prominent moraine ridges (n = 16) and large, isolated erratic boulders resting on bedrock (n = 9), from five sites. The samples were prepared at the Surface Exposure Laboratory of the Institute of Geological Sciences at the University of Bern (after Akçar et al., 2012), for the accelerator mass spectrometer (AMS) analysis of cosmogenic ^{10}Be at ETH Zürich following standard procedures (Kubik and Christl, 2010; Akçar et al., 2012; Christl et al., 2013). Ages were calculated using the Calculators formerly known as the Cronus Earth Calculators (Balco et al., 2008), v3.0.2, constants v2020-08-26, the LSDn scaling scheme (Lifton et al., 2014), and the Scandinavian ^{10}Be production rate calibration (Stroeven et al., 2015), assuming zero erosion (Tables 1 and S1). Published ages were re-calculated following the same procedure (Table S2). We additionally provide apparent ages calculated using the global ^{10}Be production rate from Borchers et al. (2016), which yields ca. 4.2% younger ages (Peltier et al., 2015; Tables S1 and S2). We primarily discuss the ages based on the Scandinavian calibration (Table 1). Correcting for elevation changes following glacial isostatic adjustment (GIA), using the ICE-6G ice model (Peltier et al., 2015), would increase the ages by ~2–7%. However, this procedure does not correct for atmospheric mass re-distribution which may offset isostatic effects (Staiger et al., 2007; Balco, 2019); due to this uncertainty we do not correct the ages for GIA. Owing to the lack of long-term snow cover thickness records, we did not attempt to correct exposure ages for snow cover, but we note that this could lead to underestimation of exposure ages by ca. 5–7% (Andersen et al., 2018; Lane et al., 2020). ^{10}Be-ages of glacially transported boulders are known to be notoriously affected by cosmogenic nuclides inherited from exposure prior to final deposition (Heyman et al., 2011; Romundset et al., 2017; Prud'Homme et al., 2020). Based on an evaluation of a large dataset of new and previously published ^{10}Be-ages from the Gudbrandsdalen region, as well as a comparison with the chronology obtained from other methods in this study, deglaciation ages older than 12.0 ka are considered as outliers due to nuclide inheritance (see Section 5.1). Ice sheet thinning rate regression analysis was performed using MATLAB codes from Jones et al. (2019), weighted external uncertainty of samples (1σ),

Table 1
^{10}Be-ages obtained from moraines and erratic boulders in this study. Apparent exposure ages are calculated using the Calculators formerly known as the Cronus Earth Calculators (Balco et al., 2008), v3.0.2, constants: 2020-08-26, the LSDn scaling scheme and the Scandinavian ^{10}Be production rate from Stroeven et al. (2015), assuming zero erosion. Further details are given in Table S1.

Locality	Sample ID	Elevation	Exposure age	Internal unc.	External unc.
		m a.s.l.	ka	kyr	kyr
Gjelutbotn	LORD-1	1528	15.1	0.4	1.0
Gjelutbotn	LORD-2	1529	14.3	0.3	0.9
Gjelutbotn	LORD-3	1529	15.2	0.3	1.0
Gjelutbotn	LORD-4	1510	11.3	0.4	0.8
Gjelutbotn	LORD-5	1498	10.9	0.4	0.8
Langranden	DOMB-1	1169	12.9	0.4	0.9
Langranden	DOMB-2	1070	10.8	0.4	0.8
Langranden	DOMB-3	1095	14.0	0.5	1.0
Langranden	DOMB-4	1120	18.0	0.5	1.2
Langranden	DOMB-5	1059	11.6	0.4	0.8
Langranden	DOMB-7	1085	11.3	0.4	0.8
Knutsmorka	SORP-1	307	10.5	0.4	0.8
Knutsmorka	SORP-2	308	10.8	0.5	0.8
Knutsmorka	SORP-3	306	10.5	0.5	0.8
Knutsmorka	SORP-4	305	11.4	0.4	0.8
Knutsmorka	SORP-5	305	10.2	0.5	0.8
Knutsmorka	SORP-5A	305	10.7	0.5	0.8
Høgranden	ROMS-1	1122	13.2	1.6	1.8
Høgranden	ROMS-2	1122	13.8	0.4	0.9
Høgranden	ROMS-3	1101	11.4	0.5	0.8
Høgranden	ROMS-4	1104	12.4	0.3	0.8
Høgranden	ROMS-5	1106	11.0	0.3	0.7
Gålåflatin	GALA-1	819	10.9	0.3	0.7
Gålåflatin	GALA-2	825	10.9	0.3	0.7
Gålåflatin	GALA-3	814	11.0	0.5	0.8

and 10.000 iterations.

3.2. Lake sediment analyses

The Gudbrandsdalen valley is a typically U-shaped valley with steep sides. Most of the valley floor is covered by thick alluvial or glaciolacustrine infill. Lakes in bedrock basins are therefore rare within the trunk valley and occur only near major steps in the valley longitudinal profile, where surficial cover often is sparse. We cored two basins located in such areas, the lake Svarttjønne near the main drainage divide at Lesjaskog in the northwest and a bog at Hardvollsmorka near Vinstra in the southern part of our field area (Fig. 2). In addition, we targeted the two lakes Åbortjønna and Kvitbergstjønna, located at higher elevations southwest of Vinstra. The Hardvollsmorka bog was cored in summer using a Russian peat corer (Jowsey, 1966), whereas the lakes were cored from the winter ice, using a piston corer modified from Nesje (1992). The lakes were cored with the purpose to obtain (minimum) ages for the deglaciation and to date the ice-dammed lake Store Dølasjø. We collected several cores from transects across each basin, each time aiming to penetrate as deep into the sedimentary sequence as possible. All samples were transported to the sediment laboratory at NGU and stored at about 4 °C for further analysis. The cores were split, and the sediment texture and lithology were described before scanning for magnetic susceptibility and imaging. One-cm thick subsamples were collected from levels interpreted to represent the earliest ice-free conditions, wet-sieved at 250-μm and carefully cleaned under a stereo microscope. The sediments were analysed for macrofossil content and plant remains were identified and picked for radiocarbon dating. The samples were dried overnight at 50 °C, packed in sterilized vials and sent to the Poznan Radiocarbon Laboratory, Poland. The radiocarbon measurements (Table 2) were calibrated using the computer software OxCal v.4.4 (Bronk Ramsey, 2009) with the IntCal20 dataset (Reimer et al.,

Table 2
Radiocarbon dates from lake sediments, obtained in this study.

Laboratory number	Basin	Depth below surface (cm)	Material dated	Sample weight (mg)	Radiocarbon age (a BP)	Calibrated age (a BP, 2σ)	Weighted average (μ)
Poz-98472	Åbortjønna, Vinstra	1130	Pinus needles, Betula leaf fragment	17	7940 ± 50	8990–8600	8800
Poz-98473	Åbortjønna, Vinstra	1140	Small twig	10	8430 ± 40	9540–9310	9460
Poz-98474	Åbortjønna, Vinstra	1142	Pinus needles	16	8590 ± 50	9690–9480	9570
Poz-98475	Åbortjønna, Vinstra	1142	Leaf fragments	21	8680 ± 50	9890–9530	9650
Poz-98476	Åbortjønna, Vinstra	1144	Salix herbacea leaf, Pinus needles	15	8900 ± 50	10 200 - 9780	10 020
Poz-98477	Åbortjønna, Vinstra	1146	Pinus needles, Betula leaves and scales	22	9130 ± 50	10 490 - 10 200	10 310
Poz-98466	Kvitbergstjønna, Vinstra	493	Twig	140	7050 ± 50	7980–7750	7870
Poz-98467	Kvitbergstjønna, Vinstra	507	Cortex pieces	27	7790 ± 50	8700–8420	8560
Poz-98468	Kvitbergstjønna, Vinstra	527	Cortex pieces	7,5	8460 ± 50	9540–9320	9480
Poz-98469	Kvitbergstjønna, Vinstra	527	Twig	35	8410 ± 50	9540–9290	9430
Poz-98471	Kvitbergstjønna, Vinstra	527	Twig	172	8410 ± 50	9540–9290	9430
Poz-82905	Hardvollsmorka, Vinstra	365–370	Mosses	5	8920 ± 50	10 220 - 9820	10 040
Poz-82906	Hardvollsmorka, Vinstra	365–370	Mosses	9	8900 ± 50	10 200 - 9780	10 020
Poz-98485	Svarttjønne, Lesja	1135	Betula nana seed, mosses and twigs	3	8850 ± 50	10 170 - 9710	9950
Poz-98556	Svarttjønne, Lesja	1136	Salix leaf, Juniper needle, leaf and twig fragments	10	9010 ± 50	10 250 - 9910	10 160
Poz-98557	Svarttjønne, Lesja	1137	Twigs and leaves	6	9100 ± 50	10 480 - 10 180	10 270
Poz-98559	Svarttjønne, Lesja	1140	Single twig with cortex	8	8950 ± 60	10 240 - 9890	10 060
Poz-98560	Svarttjønne, Lesja	1140	Betula nana seeds, various twigs	8	9210 ± 50	10 510 - 10 240	10 370
Poz-98561	Svarttjønne, Lesja	1141	Single large twig with cortex	27	9120 ± 50	10 490 - 10 190	10 300
Poz-98486	Svarttjønne, Lesja	1147	A Betula nana leaf, mosses	9	9210 ± 50	10 510 - 10 240	10 370
Poz-98562	Svarttjønne, Lesja	1148	Ericaceae, Betula nana seeds	8	9220 ± 50	10 550 - 10 240	10 380

2020). Using the P_Sequence method described by Bronk Ramsey (2008), we applied Bayesian age-depth modelling to the radiocarbon dates from two lake basins.

3.3. Mapping of ice-dammed lakes and meltwater features

We used high-resolution LiDAR-based elevation data (retrieved from hoydedata.no) to identify shorelines, measure their elevations, and make correlations. In this way we mapped the extent of former ice-dammed lakes (IDLs), as well as their configuration in relation to the thinning ice sheet, similar to Høgaas and Longva (2018) and Regnéll et al. (2019). IDL shoreline landforms were distinguished from similar morphological features, such as lateral meltwater channels, by their long and near-horizontal extent, as well as the clear relation to a former spillway across a topographic saddle point. Geomorphological mapping was carried out in ESRI ArcMap, using shaded relief images generated from a 1-m resolution digital elevation model (DEM) derived from airborne LiDAR data or photogrammetric image matching. Shaded relief images were produced with different solar azimuths (45°, 315°, 360°), solar angles (30°, 45°) and terrain exaggerations to reduce the risk of methodological bias. Measured shoreline elevations (n = 191) from the Store Dølasjø provide the basis for reconstructing a tilted IDL surface in GIS using the "Kriging" interpolation tool. Shoreline altitudes were measured on the very frontal part of the shoreline or delta features. Beach ridges were avoided for shoreline altitude measurements, as the relation between ridge height and lake level is spatially variable. The IDL shoreline altitudes were rounded off to nearest meter and used for constructing linear trendlines that represent the tilted shorelines. The tilt was statistically calculated based on linear regression and the shorelines were subsequently projected to a profile line that is oriented perpendicular to the mapped isobase direction of the Store Dølasjø shoreline. The Store Dølasjø isobase direction found in this study is nearly identical to the Younger Dryas marine shoreline isobase direction of ca. 33° at the Møre coast (Svendsen and Mangerud, 1987). Based on this relation, we assume that a common isobase direction represents all the IDLs mapped in this study (see Section 5.2). Through comparison with the chronology of the marine shoreline gradient, approximate ages for the IDLs were inferred and added to the chronology of ice-sheet thinning. The reconstructed palaeosurface of the Store Dølasjø IDL was compared to a 10-m resolution DEM of the modern terrain, to calculate the water volume of this by-far biggest and deepest of the four mapped IDLs.

In selected areas, we also mapped lateral meltwater channels, that are interpreted to have formed along the ice margin, by meltwater abrasion of the substrate in combination with accumulation of glacio-fluvial sand and gravel (Mannerfelt, 1945). The meltwater channels

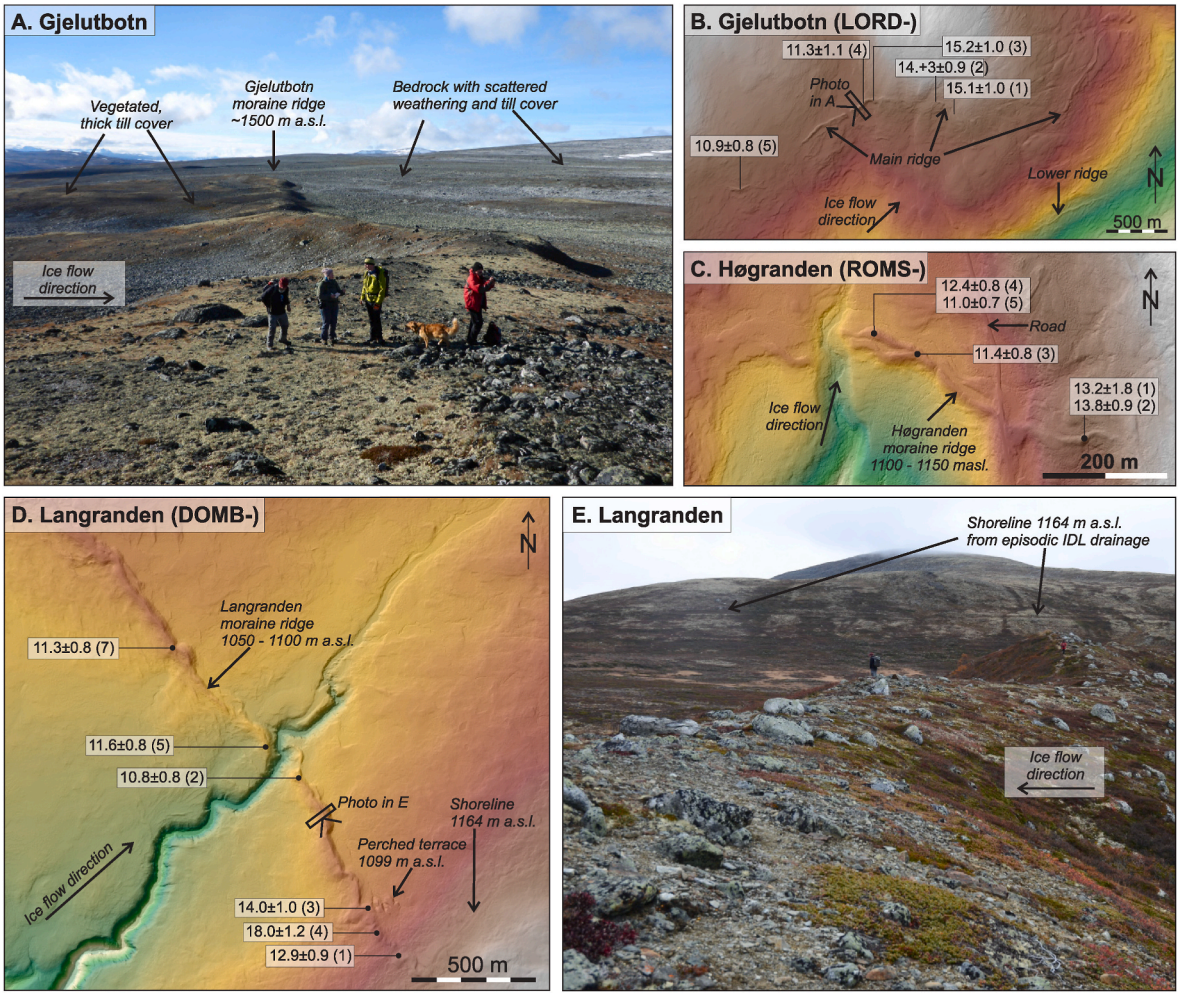

Fig. 3. A. Photo of the Gjelutbotn moraine ridge in Lordalen, marked in Fig. 2. B. Sample sites and obtained ages (including external uncertainties) from the Gjelutbotn moraine (Fig. 2). The sample number (LORD-) is given in brackets. Two samples assumed to be unaffected by inheritance are written in bold. C. Sample sites and obtained ages from the Høgranden moraine ridge in Romsdalen (Fig. 2). The sample number (ROMS-) is given in brackets. Two samples assumed to be unaffected by inheritance are written in bold. D. Sample sites and obtained ages from the Langranden moraine ridge in Lesja (Fig. 2). The sample number (DOMB-) is given in brackets. The youngest sample DOMB-2 is assumed to be unaffected by inheritance. E. Photo of the Langranden moraine ridge.

form extensive, often clearly visible lines in the mountain sides, that are dipping in the direction of former drainage and delineate the former ice sheet surface. The extent and inclination of certain sets of meltwater channels have been found, using digital elevation models and derived hillshade images.

4. Results and interpretations

4.1. Cosmogenic ^{10}Be exposure dating

We have dated boulders from three large moraine ridges in the northern part of the study area, and erratic boulders from two sites in the southern part (Fig. 2). In Gjelutbotn north of the valley Lordalen (Figs. 2 & 3A), a mostly continuous, lateral moraine ridge can be traced over a distance of 5.5 km. The ridge is 5–15 m high and about 20 m broad, and is located slightly above 1500 m a.s.l. These are among the highest situated lateral moraines in Norway, and they were deposited from the south, by ice flowing from Jotunheimen towards Romsdalen (Fig. 2). The moraine belt coincides with the transition from bare bedrock with blockfields and patchy till above, to thick and continuous till cover below (Tollan, 1963; NGU, 2023). We sampled five boulders (0.5–1 m high), which are resting at the crest of the ridge (Fig. 3B, Tables 1 and S1). The two ages 11.3 ± 0.8 ka (LORD-4) and 10.9 ± 0.8 ka (LORD-5) are considered to represent the age of ridge deposition and stabilization, with an arithmetic mean age of 11.1 ± 0.5 ka. The remaining ages are older and considered as outliers (see Section 5.1). Other, more scattered

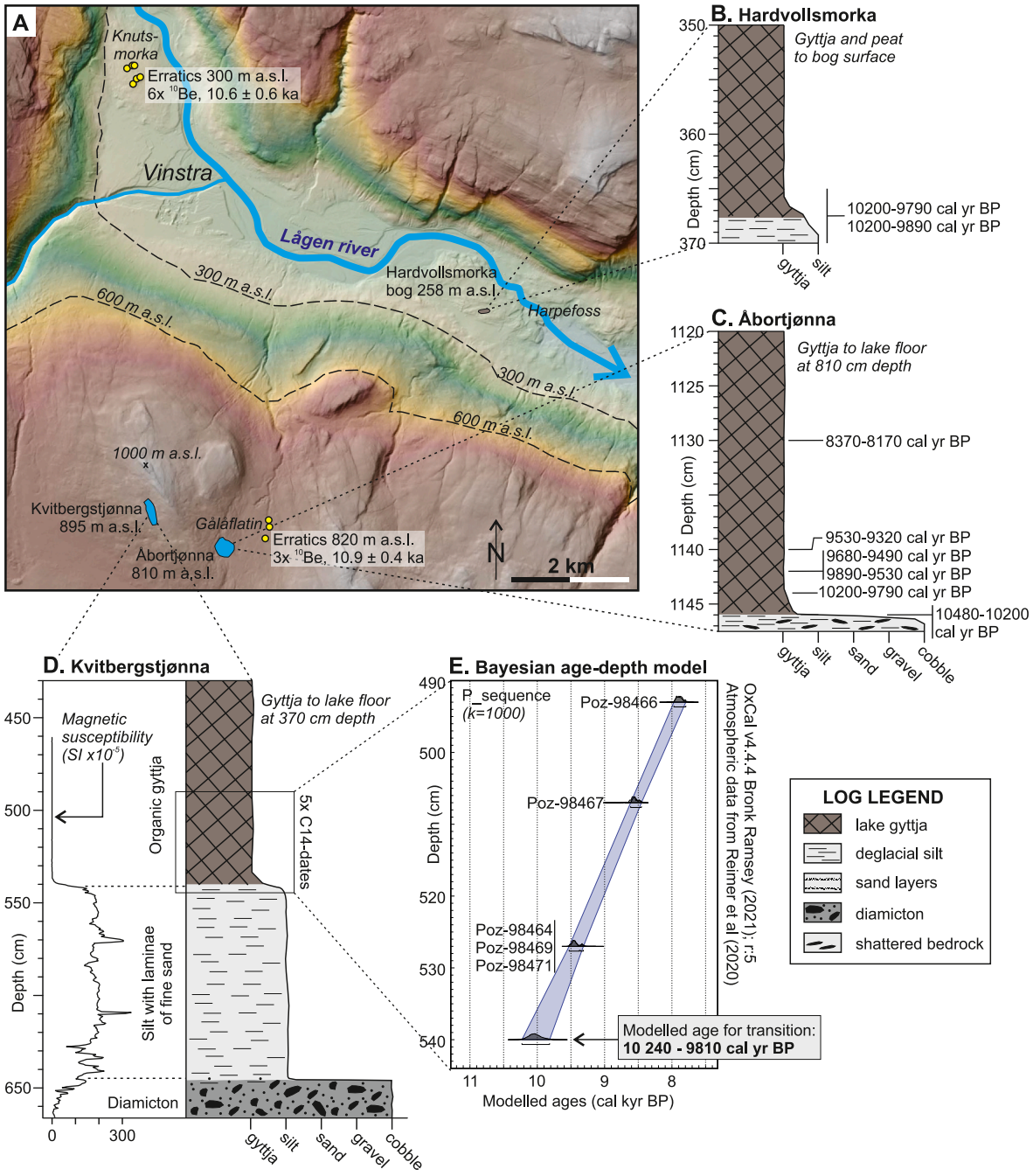

Fig. 4. A. The area near Vinstra, showing the location of sample sites for lake sediments and erratic boulders. B. The sediment record of the Hardvollsmorka bog basin at 258 m a.sl. C. The sediment record of Lake Åbortjønna at 810 m a.s.l. D. The sediment record of Lake Kvitbergstjønna at 895 m a.s.l. E. Age-depth model for the lower part of the Kvitbergstjønna sequence.

moraine ridges also occur at lower elevations in Lordalen, e.g., at around 1380 m a.s.l. as shown in Fig. 3B.

There are several lateral moraines at 1000–1100 m altitude along the deeply incised Romsdalen (Fig. 1). We sampled five boulders at the ridge named Høgranden, which crosses a tributary, hanging valley on the northern side of upper Romsdalen (Figs. 1 & 3C, Tables 1 and S1). The moraine is predominantly composed of large, stacked boulders. Two of the boulders yielded Early Holocene ages of 11.0 ± 0.7 ka (ROMS-5) and 11.4 ± 0.8 ka (ROMS-3), with an arithmetic mean age of 11.2 ± 0.5 ka. The chronology of the ice-dammed lakes indicates an age of 11.5 ka for Høgranden, i.e., overlapping with the two youngest ^{10}Be-ages. A major moraine ridge named Langranden is located at 1050–1100 m a.s.l. and crosses the wide valley of Grøndalen in the eastern part of Lesja, near Dovrefjell (Fig. 2). The ridge is 2.5 km long and rises for the most 20–30 m above the surroundings. Boulders higher than 1 m are scattered along the ridge crest. We sampled six (Tables 1 and S1), from which the three ages 10.8 ± 0.8 ka (DOMB-2), 11.6 ± 0.8 ka (DOMB-5) and 11.3 ± 0.8 ka (DOMB-7), give an arithmetic mean age of 11.2 ± 0.6 ka which agrees with the chronology of the ice-dammed lakes and represents the age of the Langranden moraine.

We sampled three large erratic boulders that rest on bedrock at Gålåflatin ca. 820 m a.s.l., just south of Vinstra (Fig. 2, Tables 1 and S1). The three boulders yielded ages of 10.9 ± 0.7 ka (GALA-1 and GALA-2) and 11.0 ± 0.8 ka (GALA-3), with an arithmetic mean age of 10.9 ± 0.4 ka, representative for the age of ice sheet surface lowering below this elevation.

Knutsmorka is an isolated bedrock hill, some 400 × 300 m wide, which rises about 50 m above the floor of Gudbrandsdalen. Large erratic boulders are scattered across the hill. We consider that the boulders were first exposed when the last remnants of the glacial ice vanished from Gudbrandsdalen. Six of the boulders located near the highest part of the hill, slightly above 300 m a.s.l., were sampled (Tables 1 and S1). All six ages overlap at one standard deviation and yield an arithmetic mean age of 10.6 ± 0.6 ka, which provides an accurate age of the final deglaciation of the valley.

4.2. Lake sediment records

Åbortjønna measures about 200 × 300 m and is located at 810 m a.s.l., i.e., nearly 600 m above the adjacent valley floor of Gudbrandsdalen (Fig. 4A). We mapped the bathymetry and found that the deepest, western part of the lake has a flat bottom at around 8 m depth. Two cores were collected, both were hammered as deep as possible. We observed splintered fragments of the local bedrock phyllite near the core base, indicating that the cores comprise the full basin record since deglaciation. The longest core measured 337.5 cm and was chosen for analysis. At the base is a 2 cm thick silt with interspersed bedrock fragments (Fig. 4C). There is a short, gradual transition from silt to overlying faintly laminated, dark brown gyttja. Plant macrofossils, including needles and leaves from the primary succession of pines and dwarf birch, were carefully washed out and prepared for radiocarbon dating. A series of six samples yielded a consistent age sequence (Table 2), indicating that the onset of organic deposition took place around 10.3 cal ka BP. The age provides a minimum, and probably near accurate, age for when the ice sheet surface thinned below this elevation.

Kvitbergstjønna is located only about 1 km northwest of Åbortjønna, and at a slightly higher elevation of 895 m a.s.l. (Fig. 4A). The basin is about 300 × 100 m across and relatively shallow, with water depths of 3.7 m over a large, flat area in the middle part of the lake where two 3 m long cores were collected. Both cores showed a similar sequence with a diamicton near the base followed by more than a meter of clayey silt and on top 170 cm of gyttja (Fig. 4D). The silt is interpreted to have been deposited from glacial meltwater in a calm water and with high sedimentation rates, possibly in a small ice-marginal lake. No plant macrofossils were found at or near the conformable boundary from silt to overlying gyttja at 540 cm depth. The nearest plant remains were found 13 cm higher, at 527 cm (Table 2). Here three parallel samples; two small twigs and a piece of cortex, yielded near-identical ages around 9.4 cal ka BP. Two samples from higher levels were also dated, and all ages were used in an OxCal age-depth model assuming constant sedimentation rates (Fig. 4E). This gave an age estimate for the silt-gyttja transition of 10.2–9.8 cal ka BP, but since initial sedimentation rates of the gyttja probably were slower, this age estimate is likely somewhat young. We combine the dates from Kvitbergstjønna and Åbortjønna, and conclude that the ice sheet surface lowered below 800 m a.s.l. around 10.3 cal ka BP.

The Hardvollsmorka area constitutes a valley threshold in Gudbrandsdalen, where the Lågen River is incised in bedrock and falls about 40 m through the rapids of Harpefoss (Fig. 4A). The area is free from surficial deposits except for some scattered boulders (not sampled). The investigated bog basin, representing a palaeo-lake, is located 258 m a.s.l. and ca. 50 m above the river and thus clearly never inundated by it. The bog measures 100 × 60 m across and the maximum depth to bedrock is 370 cm. Two parallel cores were collected from the deepest part. The lowest 7 cm consists of silt, followed by 1.7 m of lacustrine gyttja capped by 2 m of peat (Fig. 4B). The deepest, silty strata hold large quantities of macrofossils characteristic for early postglacial lacustrine colonization; oogonia from the green algae *Chara*, larvae tubes from Trichoptera caddis flies and statoblasts from the bryozoan *Cristatella mucedo*. The number of well-preserved macrofossils is much reduced above the silt layers. Moss fragments were also found within the silt layers and picked from 365 to 370 cm depth in both cores. Radiocarbon dating of parallel samples from the two cores gave near-identical ages of ca. 10.2–9.8 cal ka BP and 10.2–9.9 cal ka BP (Fig. 4B, Table 2). We were not able to identify whether the mosses are of terrestrial or aquatic origin and note that if they are aquatic there is a risk that the ages are too old due to the "hard water" effect, as suggested by the occurrence of Chara in the sediments and phyllites in the local bedrock.

Lake Svarttjønne measures about 100 × 250 m and is located ca. 10 km north of the main drainage divide, in the northernmost part of the study area (Fig. 2). The lake is on a bedrock hill consisting of granitic gneisses, some 60 m above the valley floor and River Rauma (Fig. 5A). We measured water depths along several transects and found that most of the lake floor is flat and nearly 9 m deep. Two sediment cores were recovered from the central part of the lake, ca. 40 m apart. They have a similar stratigraphy with ca. 60 cm laminated, silty sand at the base, covered by nearly 2.7 m homogenous gyttja. The transition between the two units at 1148.5 cm depth below the water surface, is distinct, but with no visual indication of interrupted deposition (Fig. 5B). The sand is interpreted to have been deposited during deglaciation, by glacial meltwater drainage along the margin of the last remaining glacial ice in the area. The uppermost sand layers therefore represent the lowering of the ice-sheet surface below the elevation of the lake (631 m a.s.l.), and hence also approximately when the main water divide (610 m a.s.l.) between eastern- and western Norway became ice free. A series of eight samples of well-preserved plant macrofossils were carefully picked from different levels within a 13-cm long interval of the lake record, across the transition from sand to gyttja (Fig. 5C; Table 2). Leaves and seeds from heather (Ericaceae) and dwarf birch (*Betula nana*), as well as well-preserved mosses are common. The deepest occurring plant fragments were found within the uppermost sand layers, suggesting that vegetation was established around the lake near simultaneously with the final episodes of sand deposition. The series of eight radiocarbon ages gave consistent results and suggest that woody plants grew near the lake, and apparently close to the ice margin, at 10.4 cal ka BP (Fig. 5C).

4.3. Mapping of large ice-dammed lakes

Digital elevation models covering the entire study area have been examined with the aim to detect shoreline features from temporary ice-dammed lakes (IDLs), that formed during the deglaciation. Meltwater was commonly ponded along the ice margin, but only in topographically

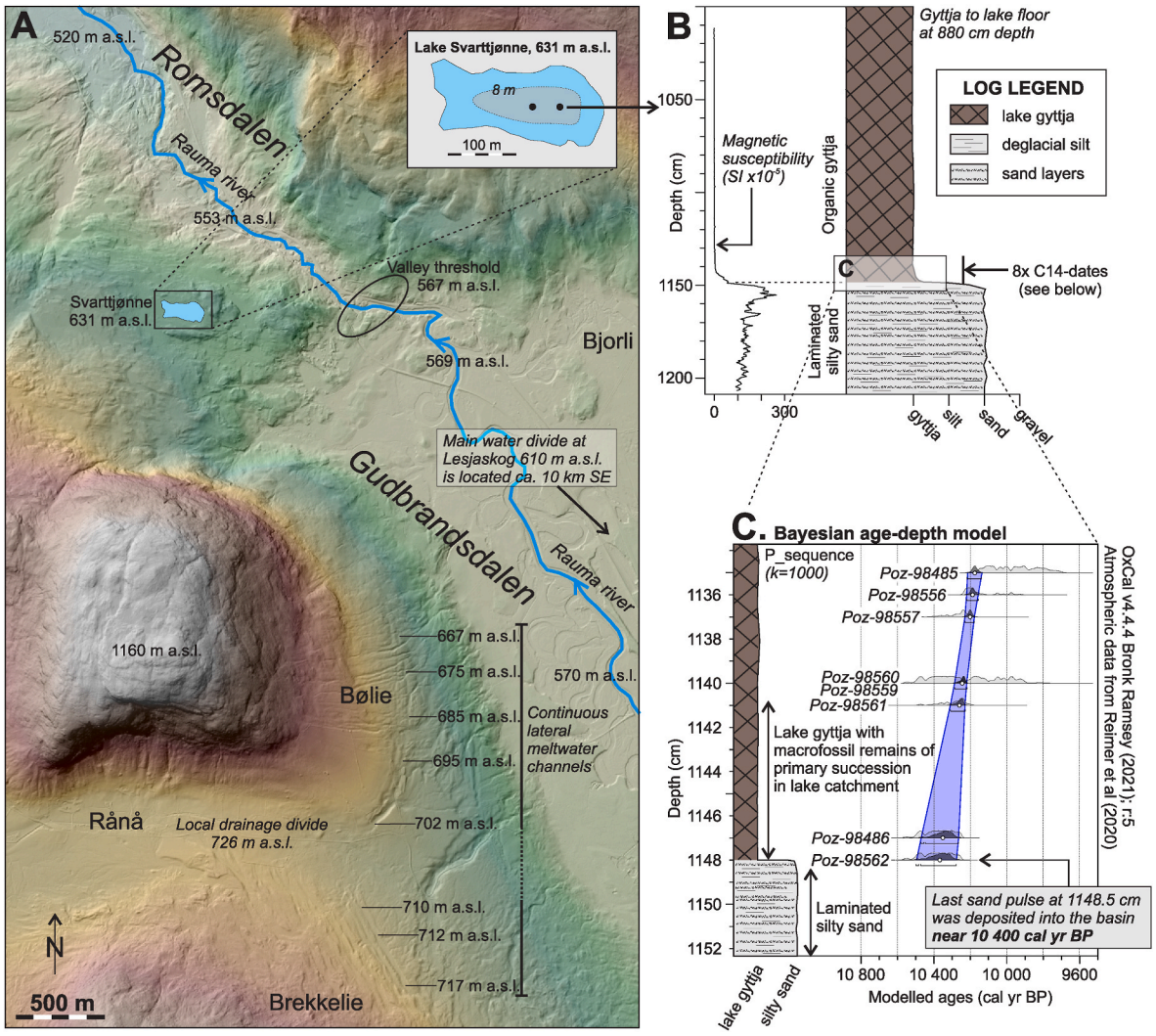

Fig. 5. A. The study area ca. 10 km north of the main drainage divide at Lesjaskog, showing the location of the Svarttjønne lake basin and details on local geomorphology discussed in the text. B. The sediment record of Svarttjønne. C. Bayesian age-depth model for the transition from glacially derived meltwater deposits to organic lake gyttja.

favorable locations this led to formation of larger IDLs, that existed for sufficient time to allow formation of shoreline landforms that are still preserved. The mapped extent of four such large IDLs are presented in this study, but we note that traces from smaller IDLs were also observed. The mapping includes the by-far largest and previously known Store Dølasjø (Garnes and Bergersen, 1980), which left distinct shoreline features along the sides of both the main and tributary valleys of Gudbrandsdalen (Fig. 2). The shoreline of the Store Dølasjø is represented by glaciofluvial deltas, terraces, and beach ridges, as well as laterally extensive wave-cut scarps in till. For large parts of the area, the shoreline is continuous over many kilometers. Our mapping largely confirmed the work of Garnes and Bergersen (1980), and resulted in a precise reconstruction of the Store Dølasjø IDL, which at its full extent had a surface area of ca. 480 km^2 and a volume of ca. 80 km^3. This makes it larger than the biggest lake in Norway today (Lake Mjøsa, 362 km^2; Fig. 1), but less than half the size of the largest deglacial IDL in Norway, the Nedre Glomsjø IDL (Fig. 1; Høgaas and Longva, 2018).

The Store Dølasjø was confined in the north by the main drainage divide at Lesjaskog, and in the south by an ice dam a few km north of Vinstra. Much of the Store Dølasjø IDL was several hundred meters deep (Figs. 2 & 9A). The shallowest part of the lake was found in the northern branch occupying Lesja and Dovre, where today thick and extensive glaciolacustrine silt deposits cover the valley floor (Reusch, 1910; Holmsen, 1965; NGU, 2023). Very high rates of silt deposition probably dominated this part of the IDL, owing to a lower energy regime and excess of suspended sediments from glacial meltwater. Scattered pebbles and boulders that occur within and on top of the thick glaciolacustrine silt are probably ice-rafted debris, deposited from icebergs. For the northernmost 15 km of the reconstructed IDL, between Lora and Lesjaskog (Fig. 2), no clear shoreline features have been found. Here the valley floor is covered by thick glaciofluvial gravel and numerous dead-ice landforms such as eskers, kames, kettle holes and kame terraces. Remaining, stagnant and partly buried ice bodies probably directed the drainage and prohibited formation of clear shoreline features in this very shallow part of the lake. A western branch of the IDL occupied most of Ottadalen (Fig. 2), but the shorelines disappear abruptly in Skjåk and near the mouth of the tributary valley Bøverdalen (Fig. 2). Apparently, remaining remnants of the ice sheet blocked these valleys, but no ice-marginal deposits from this stage of the deglaciation have previously been described (Sollid and Trollvik, 1991), or discovered in this study through surveys of digital elevation models.

The three other IDLs, mapped at higher elevations in the northern part of the study area, have not previously been described. Continuous wave-cut scarps delineate an IDL, mostly 2–300 m deep and with a surface area of ca. 40 km^2, in the Brøstdalen valley (NW corner of Fig. 2). The lake formed between an ice tongue in Romsdalen and a saddle point

in the northeast end of the IDL, where distinct meltwater channels are found. The ice tongue was an outlet glacier from the remnants of the Scandinavian Ice Sheet centered over Jotunheimen and flowing towards the north, across the Ottadalen valley.

Another IDL, with a surface area of ca. 28 km^2 and mostly less than 100 m deep, was located in the Grøndalen valley near Dovrefjell (Fig. 2). The shoreline is seen as wave-cut abrasion scarps in many locations, and it correlates with a spillway at 1225 m a.s.l., with channels showing drainage across the main water divide to Drivdalen in the north. A distinct network of meltwater channels and eskers in the Dalsida valley west of the Grøndalen IDL (Fig. 2), show that it probably drained progressively along and beneath the ice margin during ice sheet thinning. Scattered shoreline marks also occur at lower elevations in Grøndalen. These were formed during later and briefer IDL-stages, partly in conjunction with formation of the Langranden moraine (Fig. 3E). The Langranden moraine thus post-dates the main Grøndalen IDL. It should be noted that the area of Lesjøtelet northwest of Grøndalen (Fig. 2), although topographically favorable for damming of a large IDL between the ice margin and the main drainage divide, probably did not host any IDL for a significant period of time. Distinct meltwater channels at 1375 m a.s.l. represent drainage across the main drainage divide towards Drivdalen during the deglaciation, but no correlative shoreline features have been found.

In the Dalsida tributary valley, a 25 km^2 large and mostly 100–150 m deep IDL is reconstructed (Fig. 2), based on almost continuous shoreline features (perched deltas, terraces and wave-cut abrasional scarps). The Dalsida IDL was blocked in the south-eastern end by remaining glacial ice in the main valley of Gudbrandsdalen, where the shoreline suddenly disappears at 877 m a.s.l. The IDL drained towards the fjord valley Eikesdalen in the northwest (Fig. 2), in a spillway at 859 m a.s.l. across the main drainage divide of Norway.

5. Discussion

5.1. Chronology and rates of ice-sheet thinning

We augment the new ^{10}Be-dates from Gudbrandsdalen in this study with a compilation of published cosmogenic exposure data from the adjacent mountain areas of Reinheimen and Blåhøe (Fig. 2; Table S2). The ^{10}Be dataset from Reinheimen (Andersen et al., 2018) was collected from elevations 1826–1068 m a.s.l., at and near the Kjølen mountains (Fig. 2) and is comprised of 40 bedrock samples, 4 samples from blockfield boulders, and 2 samples from glacial erratics. The Blåhøe dataset was collected from ca. 1600–1100 m a.s.l. and consists of 20 bedrock samples and 7 samples from glacial erratics, 7 of these samples were collected within the summit blockfield (Linge et al., 2006; Goehring et al., 2008). The application of surface exposure dating in various deglaciation settings has shown that nuclide inheritance from previous exposure is common (e.g., Applegate et al., 2012; Mangerud et al., 2013; Briner et al., 2014; Svendsen et al., 2015; Romundset et al., 2017; Prud'Homme et al., 2020), probably due to shallow glacial erosion (< a few meters). This is also the case for the previous studies near Gudbrandsdalen, as well as for the ^{10}Be-dated localities in the present study, as cold-based ice cover can be expected in areas near the former ice divide (Stroeven et al., 2016).

To assess the level of inheritance, we combine the 73 ages from Reinheimen and Blåhøe (Table S2) with the 25 new ages from this study (Tables 1 and S1), in a probability density plot using the PCAAT software (Dortch et al., 2022). After excluding four ages older than 35 ka, the distribution of the remaining 94 ages shows that while many ages pre-date the LGM and are clearly too old, a total of 54 ages cluster around 11.1 ± 0.9 ka (Fig. 6A). Based on the age distribution (Figs. 6 and 7A) and the two other, independent datasets (i.e., the ice-dammed lake chronology and the radiocarbon chronology based on cored lakes), we consider that the deglaciation post-dates 12.0 ka, and samples giving older ages contain various amounts of inherited nuclides from previous exposure. For estimates of the deglaciation of the individual sites, ages >12.0 ka are thus regarded as outliers (Fig. 6B).

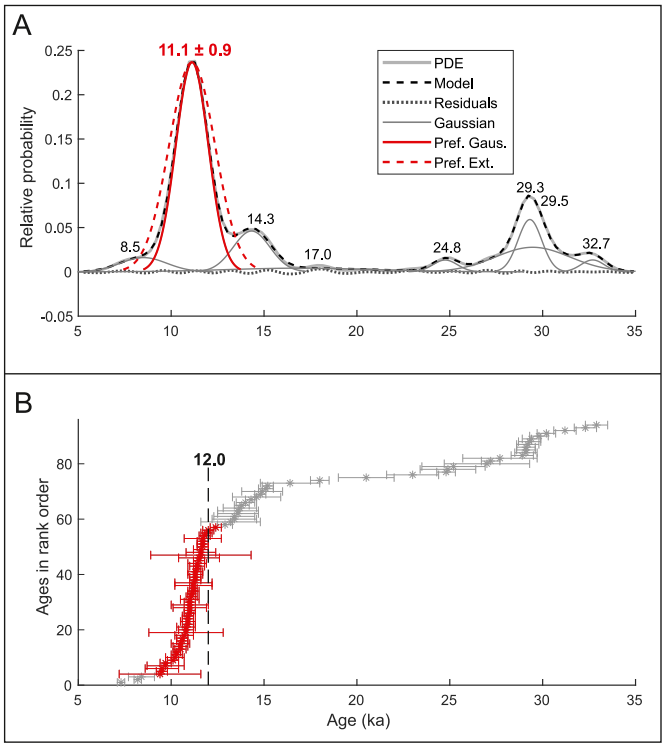

Fig. 6. A. Camel plot of 43 deglaciation ages from Reinheimen (Andersen et al., 2018), 26 deglaciation ages from Blåhøe (Goehring et al., 2008) and 25 new ages from moraines and erratic boulders in this study, produced with the PCAAT software (Dortch et al., 2022), together 94 samples, of which 54 of the ages cluster around 11.1 ± 0.9 ka (red curve), reflecting the timing of rapid ice-sheet thinning below mountain summits in the area. B. The distribution of ages in rank order. Ages older than 12.0 ka are defined as outliers and rejected from our chronology.

Also relevant to the deglaciation in Gudbrandsdalen, Lane et al. (2020) published a dataset of 14 ^{10}Be ages from boulders and 7 from the bedrock surface, spread at elevations 1800–1358 m a.s.l. near Mt. Snøhetta (Fig. 2, Table S2). 15 of their ages cluster around 11.4 ± 0.4 ka, in agreement with the datasets from Reinheimen and Blåhøe. The ^{10}Be ages from Snøhetta are plotted for comparison but were not included in the regression analysis due to the more northerly location. However, they fit well into the pattern (Fig. 7). Marr et al. (2019) reported ^{10}Be ages of two additional samples from Blåhøe, both are older than 20 ka and have not been included in this compilation.

Given the results of the ^{10}Be-dating, in combination with the independent chronologies obtained from the shoreline tilts of the IDLs and the radiocarbon-dated lake records, we conclude that the final ice-sheet thinning below mountain summits and gradual exposure of the landscape took place in the Early Holocene. Monte Carlo modelled linear thinning rates for Gudbrandsdalen (Jones et al., 2019; Small et al., 2019), are estimated from the datasets from Blåhøe (Linge et al., 2006; Goehring et al., 2008), Reinheimen (Andersen et al., 2018), and from the new ^{10}Be-dated localities in this study, excluding the outliers. The thinning rate estimates range from 1.7 to 5.8 m yr^{-1} (one standard deviation; 68%) and 1.3–25.4 m yr^{-1} (two standard deviations; 95%) (Fig. 7A). Samples older than the thinning profile likely contain some amount of inherited ^{10}Be from exposure prior to the last glacial transport, while the high young samples could be an effect of local ice remnants, post-glacial surface cover (snow/water/till), erosion, or rotation of erratics.

Radiocarbon dates from lake cores are independent datasets against which the ^{10}Be-based thinning rate chronology can be tested.

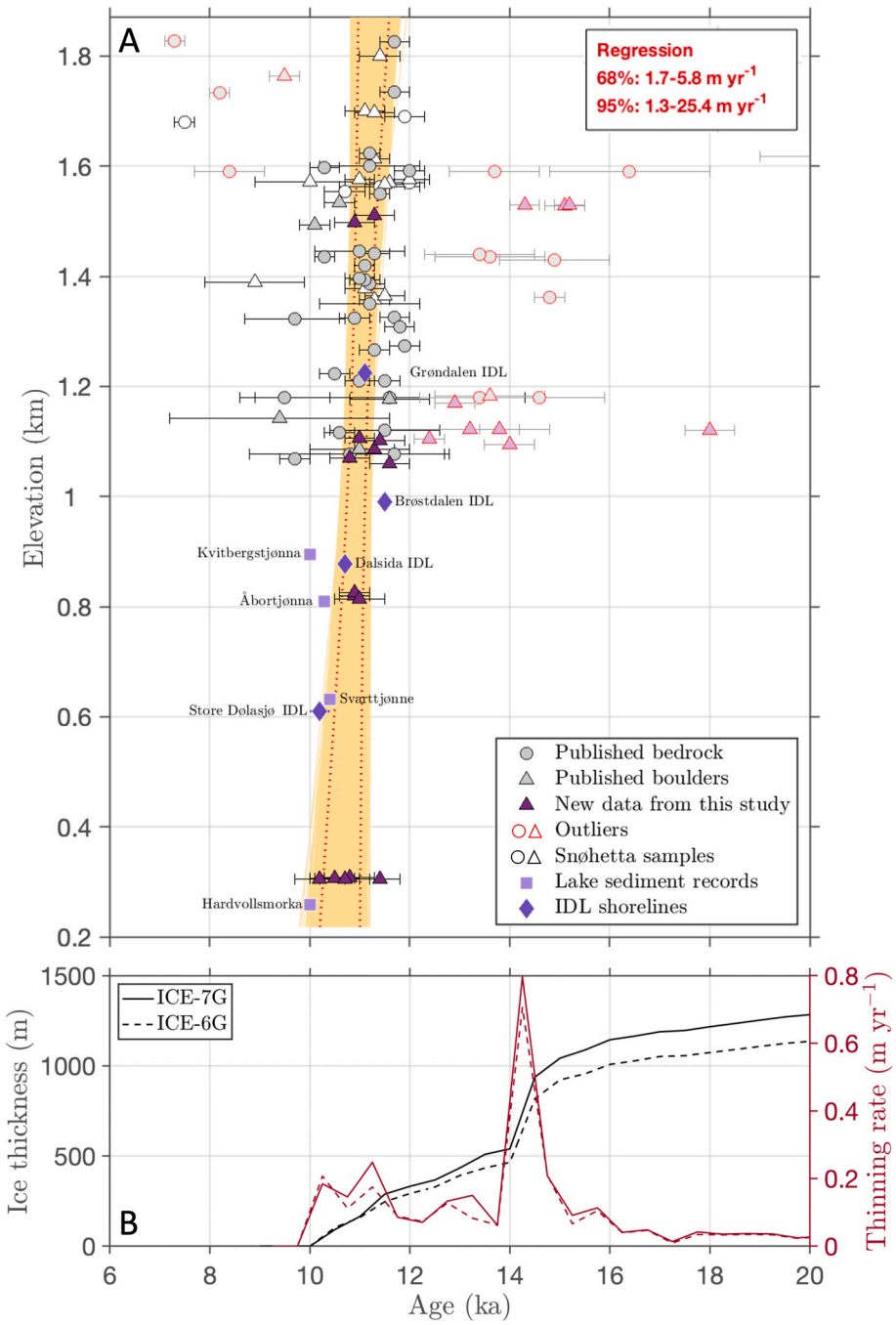

Fig. 7. A. Vertical transect of ^{10}Be apparent exposure ages in Gudbrandsdalen with Monte Carlo modelled linear thinning rate estimates (yellow area) and 95% confidence interval (red dotted lines). The thinning rate is estimated from cosmogenic ^{10}Be ages of bedrock (circles) and boulders (triangles) from Blåhøe (Linge et al., 2006; Goehring et al., 2008 incl. supplementary data), Reinheimen (Andersen et al., 2018), and from Gjelutbotn, Langranden, Høgranden, Gålåflatin, and Knutsmorka (this study). The values of the 68% and 95% confidence intervals for the best-fit linear thinning rate estimate are shown. Samples used in the regression analysis have black outlines, while samples excluded from the analysis are marked with red outlines and paler colours. All samples older than 12.0 ka are considered outliers, as are samples that are both high (>1.5 km) and young (<10 ka) and which would otherwise require a negative thinning profile slope. Cosmogenic ^{10}Be ages from near Snøhetta (Lane et al., 2020), radiocarbon dates from lake cores, and obtained ages for ice-dammed lakes (IDLs) are plotted for comparison but were not included in the regression analysis. B. Modelled ice sheet thickness and derived ice-sheet thinning rates at 62N, 9E (between Reinheimen and Mt. Blåhøe) according to ICE-6G (Peltier et al., 2015) and ICE-7G (Roy and Peltier, 2018).

Kvitbergstjønna and Åbortjønna, at elevations 800–900 m a.s.l. (Fig. 7A), yielded slightly younger ages, whereas the two lower (Svarttjønne and Hardvollsmorka) are within the error of the ^{10}Be-based thinning rate estimate, but all four are on the young side. We consider that the radiocarbon samples provide the more precise ages and thus that the ^{10}Be-ages are somewhat influenced by inheritance even if outliers are excluded.

Ages obtained from the tilted IDL shorelines (see Section 5.3) provide another independent dataset to test the thinning rate chronology. They also plot within the error of the ^{10}Be-based thinning rate estimate (Fig. 7A), except for the Brøstdalen IDL which was located ca. 50 km west of the other localities, i.e., nearer the YD ice margin, and thus does not accurately coincide with the reconstructed chronology.

The Younger Dryas ice sheet thickness at the ice divide in central parts of southern Norway has been assumed to be close to 2000 m (Hughes et al., 2016; Stroeven et al., 2016; Patton et al., 2017). Using this ice sheet thickness and a thinning period of 1600 years from the end of the Younger Dryas until the valley floor was ice free at 10 ka, gives an average thinning rate of 1.25 m yr^{-1}, showing that this ice thickness is compatible with the lower range of the ^{10}Be-derived thinning rate estimate.

Our age estimate for the disappearance of the last ice remnants in Gudbrandsdalen (~10 ka; Fig. 7A) corresponds well with the ICE-6G (Peltier et al., 2015) and ICE-7G (Roy and Peltier, 2018) models. It is, however, difficult to directly compare the modelled ice surface elevations with our data, due to the poor resolution of the topography and reconstructed ice sheet in the ICE-G models (1 × 1° grid). The main phase of ice-thinning in the ICE-G models occurs between 14.5 and 14 ka with a thinning rate of ~0.8 m yr^{-1}, followed by slower (~0.1–0.2 m yr^{-1}), and relatively steady thinning through to the Early Holocene

(Fig. 7B). As such, it seems that the ICE-G models underestimate the rate of ice-thinning following the Younger Dryas in our study region, by around an order of magnitude. Therefore, they may also underestimate the true ice-sheet thickness during the Younger Dryas. Because glacial valleys are not resolved in the ICE-G models, the thinning estimates are expected to deviate increasingly as more land areas become ice free. The thinning estimates derived from our reconstruction and the ICE-G models can therefore only be directly compared at the beginning of the Holocene, when only the highest peaks were exposed. Towards the end of the deglaciation our reconstruction shows that ice was isolated in the deepest valleys, occupying only a fraction of the total area of the landscape (and the ICE-G grid cells). For this situation only the remaining ice volumes can be compared; it is no longer appropriate to compare the ice-thickness change estimates.

5.2. Tilt of the ice-dammed lake shorelines

All the four mapped IDLs are larger than 25 km^2 and have lateral extents which make it possible to determine their present shoreline tilt, mirroring the differential postglacial uplift (Fig. 8). The orientation of the Store Dølasjø shoreline isobases can be confidently reconstructed, due to the geographical extent of the large IDL (Fig. 9A). This results in almost identical isobases as for the marine Younger Dryas (YD) shoreline at the Møre coast (Svendsen and Mangerud, 1987). There is a slight deviation of 3–4° in a more northerly direction for the Store Dølasjø isobases (Fig. 9A), which in theory could mirror the shift of ice load distribution in the Early Holocene. However, we consider this to be within the uncertainty of the isobase determination both for the Store Dølasjø and for the YD marine shoreline. Based on the near-uniform crustal uplift pattern across this region, we use a common projection

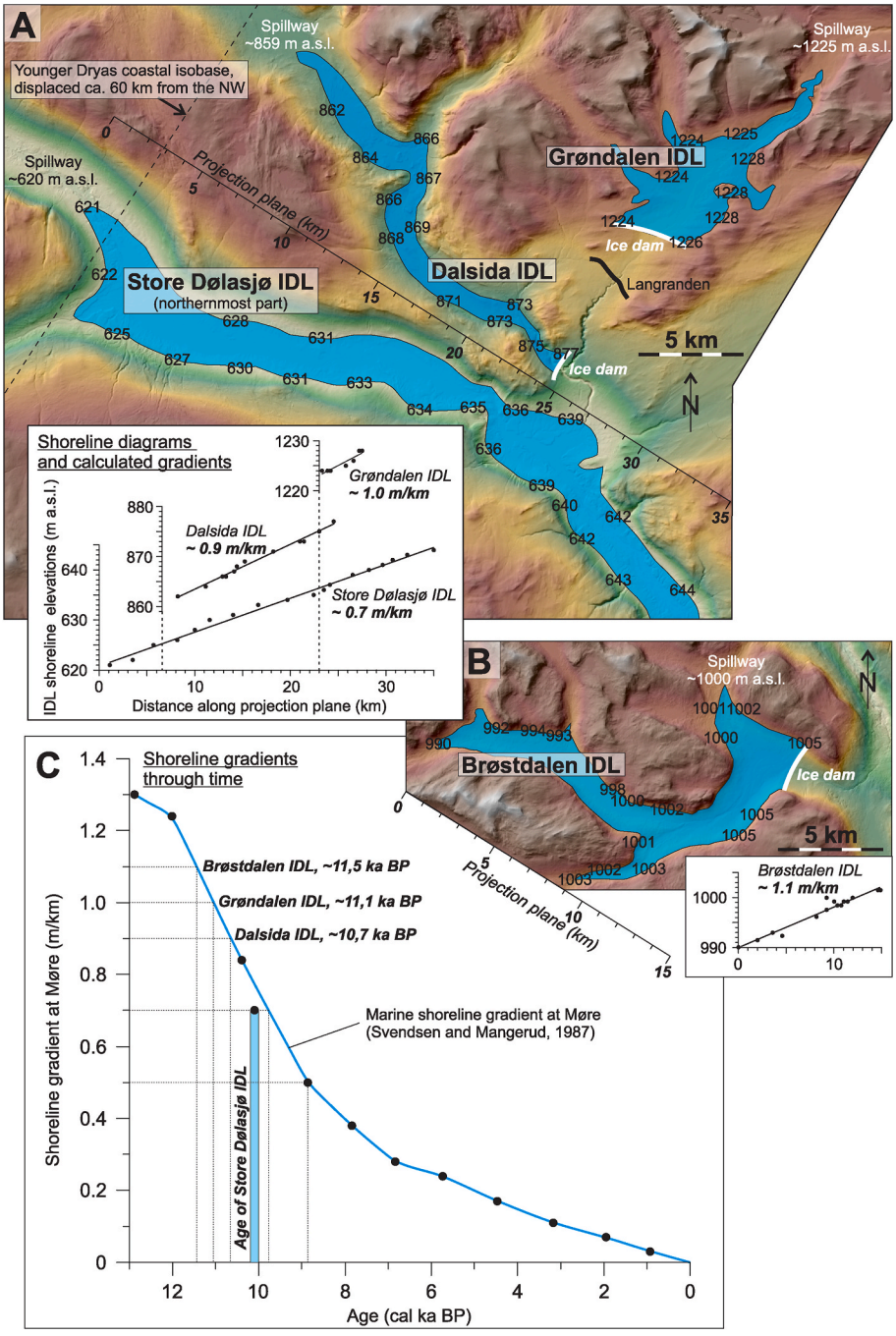

Fig. 8. A. Map showing the northern branch of the Store Dølasjø ice-dammed lake (the full lake extent is shown in Figs. 2 and 9), as well as the higher Dalsida and Grøndalen ice-dammed lakes (IDLs). Inset: Shoreline diagrams for the three lakes. B. Map and shoreline gradient reconstruction for the Brøstdalen IDL located farther west (Fig. 2). C. Shoreline gradient reconstruction from the Møre coastal area (Svendsen and Mangerud, 1987), revised to represent calibrated years (not ^{14}C-years) before present. Approximate ages of the IDLs can be inferred from their shoreline gradients. The Store Dølasjø IDL stretched much farther inland and is independently dated based on sedimentary archives from present lakes in this work.

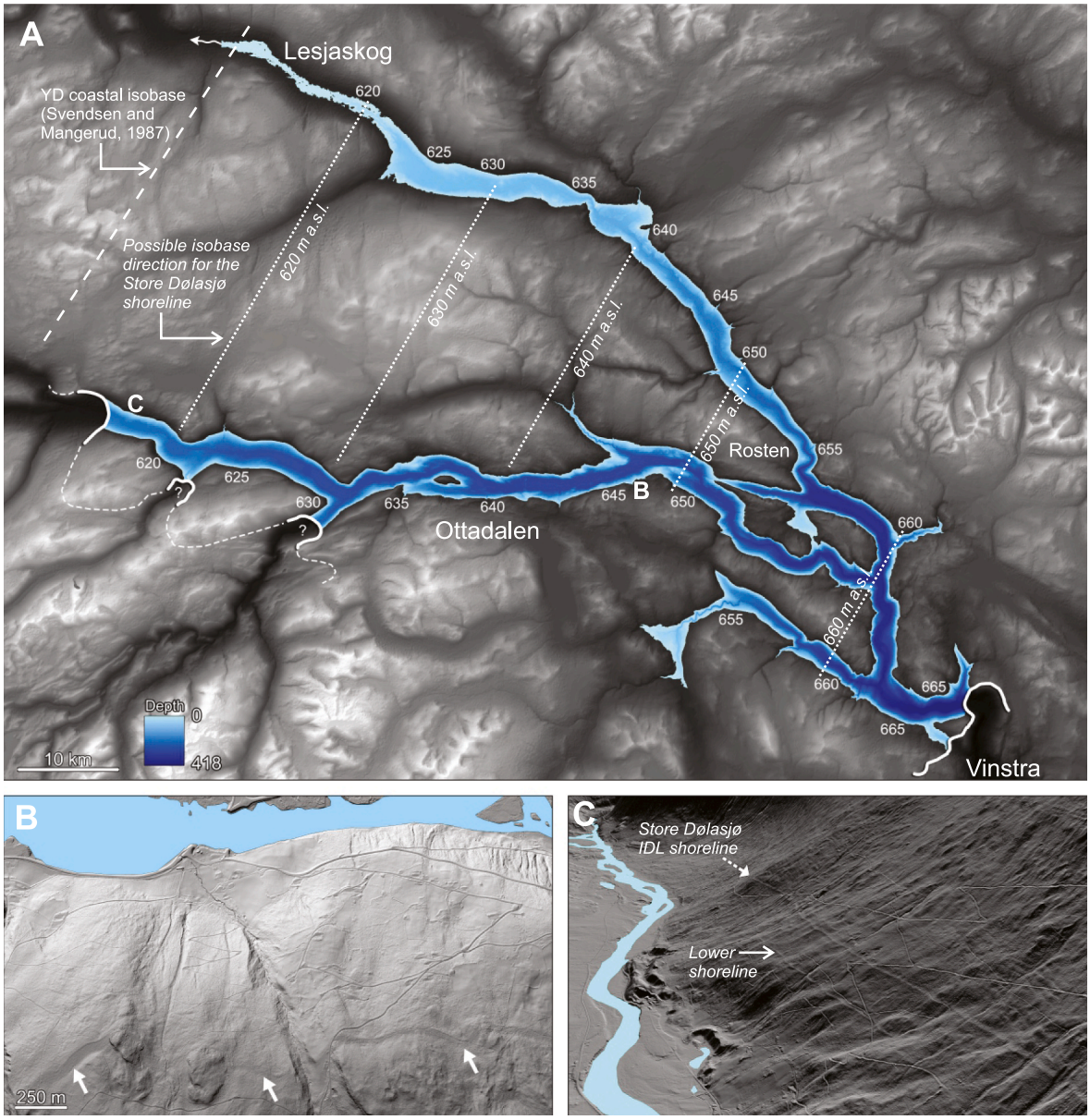

Fig. 9. A. The full extent of the Store Dølasjø ice-dammed lake, including a selection of measurements of the shoreline elevation (m a.s.l.). The measurements are used to reconstruct shoreline isobases (stippled lines) with a slightly more northerly direction than the Younger Dryas marine shoreline isobase at the Møre coast (Svendsen and Mangerud, 1987). The lake depth is also indicated, as well as suggested positions of ice sheet remnants in Gudbrandsdalen to the southeast and in Jotunheimen to the southwest. B. Details of the Store Dølasjø shoreline (white arrows), from the eastern part of Ottadalen. C. 3D view of the Store Dølasjø shoreline (shown with arrow) in Skjåk, western Ottadalen. Here, a lower level can also be seen, which is likely related to a slightly younger drainage across Øldalen near Vinstra (Fig. 2).

plane for plotting the shoreline elevations of all four IDLs (Fig. 8).

The Brøstdalen IDL shoreline rises from 990 m to 1005 m a.s.l. from west to east, yielding a tilt of 1.1 m/km, perpendicular to the isobase direction (Fig. 8B). This is slightly gentler than the Younger Dryas marine shoreline at 1.2 m/km, found along the fjords only ca. 30 km farther west (Svendsen and Mangerud, 1987). The Grøndalen IDL shoreline rises from 1224 m to 1228 m a.s.l. across the IDL (Fig. 8A), yielding a tilt of 1.0 m/km, whereas the neighbouring Dalsida IDL rises from 859 to 877 m a.s.l. and has a calculated shoreline gradient of 0.9 m/km (Fig. 8A). The Store Dølasjø IDL shoreline is tilting about 0.7 m/km in the northern part (Fig. 8A), but our mapping shows that it is significantly gentler (ca. 0.5 m/km) in the southeastern part (Fig. 9). This change can likely be explained by the location closer to the ice divide where the tilting will flatten out before tilting the opposite way on the other side of the ice divide. The variation may also be partly due to diachronous development of the Store Dølasjø shoreline from north to south, during rapidly decreasing tilt angles (Fig. 8C).

5.3. Age of the three ice-dammed lakes at higher elevations

We obtained ages for the three IDLs at higher elevations, by comparing their shoreline gradients with the change in the postglacial marine shoreline gradient at the adjacent inner Møre coast (Svendsen and Mangerud, 1987). The pattern of palaeo-shorelines reflects the ice load distribution and therefore they should be slightly curved when extrapolated over long distances, towards the former ice divide (Svendsen and Mangerud, 1987; Regnéll et al., 2019). However, Svendsen and Mangerud (1987) were not able to identify such curvature for their coastal transect of ca. 150 km. The three high-elevation IDLs in this study were located 30–70 km farther inland and we assume that the

effect of curvature is almost negligible for these sites. Comparison with the decline in marine shoreline gradient gives ages of 11.5 ka for the Brøstdalen IDL, 11.1 ka for the Grøndalen IDL and 10.7 ka for the Dalsida IDL (Fig. 8C).

The results provide tight constraints for the ages of the Høgranden and the Langranden moraines. The Høgranden is located just across the 3–4 km wide and >1 km deep Romsdalen valley, and at a similar elevation (Fig. 2) as the Brøstdalen IDL, and we consider that the moraine was formed at the same time as the IDL. The IDL shoreline age of 11.5 ka overlaps with the ^{10}Be-ages for the moraine of 11.0 ± 0.7 ka and 11.4 ± 0.8 ka. The Langranden moraine is situated between the IDLs in Grøndalen and Dalsida, both in terms of elevation and geographical location (Fig. 8A). Based on the reduction in shoreline tilt, the Dalsida IDL formed ca. 400 years later than the neighbouring Grøndalen IDL, which is located ca. 350 m higher. This provides tight age constraints between 11.1 and 10.7 ka for Langranden and supports the ^{10}Be age of 11.2 ± 0.6 ka. The IDL results show clearly that older ^{10}Be-ages from moraine boulders are affected by nuclide inheritance. We consider the uncertainty associated with the chronology based on the IDL sequence to be within 100–200 years since it is based on a consistent regional pattern, and it has high chronological resolution due to the rapid crustal uplift rates in the Early Holocene. Given the uncertainties associated with surface exposure dating, we emphasize the strength and precision of the IDL-based chronology.

5.4. Age of the store Dølasjø ice-dammed lake

The transition from glacial silt and sand to gyttja in lake Svarttjønne (631 m a.s.l.; Figs. 5 and 10) is dated to ca. 10.4 ka and this represents a time briefly before the main drainage divide at Lesjaskog (ca. 610 m a.s.l.) became ice free. The initial phase of the Store Dølasjø IDL followed soon after, when lateral lakes formed along the rapidly decaying ice sheet. The Store Dølasjø progressively grew to its full extent before it emptied, probably as a catastrophic outburst flood. A minimum age of 10.0 cal ka BP for the drainage of the Store Dølasjø, is provided by dated mosses in the basal sediments of the Hardvollsmorka bog basin near Vinstra (Figs. 4 and 10).

We conclude that the Store Dølasjø IDL existed from 10.4 to 10.0 cal ka BP (Fig. 10), but since the IDL developed progressively, much of the shoreline likely formed close to 10.0 ka BP. The shoreline gradient would suggest an age about 100 years younger (Fig. 7C). The Store Dølasjø thus existed and drained somewhat later than the Nedre Glomsjø IDL (Fig. 1), which was emptied by a catastrophic outburst flood radiocarbon dated to 10.5–10.3 cal ka BP (Høgaas et al., 2023). The radiocarbon age difference between the IDLs Nedre Glomsjø and Store Dølasjø corresponds with the difference in shoreline gradients. The Store Dølasjø shoreline is tilted 0.7 m/km for most of its extent, whereas the gradient for northern parts of the Nedre Glomsjø shoreline has been mapped to ca. 0.8 m/km (Holmsen, 1916), and thus represents a slightly older age.

At several localities in Ottadalen, a parallel shoreline was identified

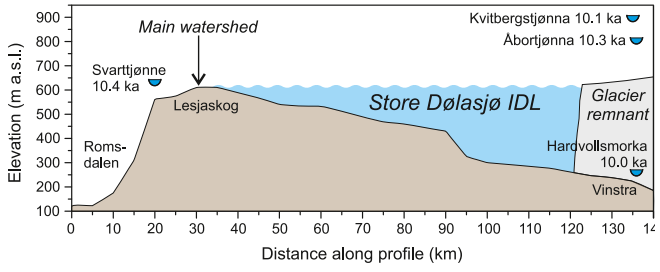

Fig. 10. NW-SE profile of the Store Dølasjø, showing the radiocarbon dated lake localities that are used to constrain the age of formation and final drainage of the ice-dammed lake.

at ca. 50 m lower elevation (Fig. 9C). The drop in elevation could possibly correspond with later drainage across a lower bedrock threshold at Øldalen near Vinstra (Fig. 2), i.e., suggesting that parts of the valley were refilled and that a shorter-lived, smaller IDL formed, after the main Store Dølasjø first emptied.

5.5. Ice-sheet configuration during the deglaciation

The margin of the Scandinavian Ice Sheet during the Younger Dryas (YD) is known along its entire periphery (Andersen et al., 1995; Hughes et al., 2016; Mangerud et al., 2023a), but its thickness has been debated (Nesje et al., 1987, 1988; Svendsen and Mangerud, 1987; Nesje and Dahl, 1990; Dahl et al., 1997; Goehring et al., 2008; Follestad and Fredin, 2011; Mangerud et al., 2011; Lane et al., 2020). The YD ice-marginal deposits are found near the fjord heads along the Møre coast (Fig. 1; Sollid and Sørbel, 1979; Aarseth et al., 1997). Mapping of glacial striae and drumlins documents that during full ice cover, the ice flowed from a dispersal centre in and east of the Jotunheimen mountains, across our field area towards Romsdalen in the northwest, and crossing Dovrefjell to the north (Fig. 2; Rekstad, 1898; Tollan, 1963; Sollid and Sørbel, 1979; Garnes and Bergersen, 1980; Hole and Bergersen, 1981; Sollid and Kristiansen, 1984; Sollid and Trollvik, 1991; Follestad and Fredin, 2011; NGU, 2023).

In this study we apply three different approaches, to reconstruct the thinning and final melting of the Scandinavian Ice Sheet in this part of Norway. The elevations and age results from our study sites are plotted along a longitudinal profile of Gudbrandsdalen from Vinstra to Lesjaskog and further along Romsdalen to the northwest (Fig. 11) and are used to reconstruct the ice sheet extent at different stages during the final deglaciation (Fig. 12). We maintain that the YD ice sheet covered the region, with the closest ice margin located in the inner fjords in the northwest (Fig. 12A). The ice sheet over Gudbrandsdalen thinned at average rates of 1.74–5.8 m yr^{-1}, over a ca. 1600-year long period in the Early Holocene. Areas closer to the YD ice margin were covered by thinner YD ice and located at lower (warmer) elevations and became ice-free first (Fig. 12B). This explains why the westernmost Brøstdalen IDL became ice free 400 years earlier than the Grøndalen IDL, despite being located ca. 225 m lower (Figs. 11 & 12B). The ice margin became increasingly dissected by expanding ice-free mountain areas, as it retreated inland. Radiocarbon-dated plant macrofossils found in basal sediments from several lakes at 1200–1300 m a.s.l. near Drivdalen north of Gudbrandsdalen (Fig. 12C), give minimum ages for local deglaciation of ca. 11.2 cal yr BP (Paus et al., 2011, 2015). Remnants of YD valley glaciers probably occupied the deep valleys well into the Holocene (Fig. 12C & D). The ice flow became increasingly influenced by topography and eventually ceased when the ice margin retreated south of the main drainage divide (Fig. 12D).

The present ice thinning reconstruction is in accordance with previous models of ice sheet geometry during deglaciation, both based on empirical data (Sollid and Sørbel, 1979; Mangerud et al., 2011, 2018; Hughes et al., 2016; Stroeven et al., 2016), as well as ice-sheet modeling (Patton et al., 2017). On the contrary, Lane et al. (2020) used ^{10}Be-ages from near Snøhetta (Fig. 2) as arguments for substantial ice sheet thinning and ice-free areas prior to the YD, but it is here shown that their ages fall within the reconstructed timeframe for ice sheet thinning presented in this paper (Figs. 7 and 11).

Our mapping of lateral meltwater channels in selected areas documents meltwater drainage along the margins of the thinning ice sheet, as mountain peaks and valley sides became exposed. The meltwater channels typically fall with gradients of 15–25 m/km, with a tendency of steeper channels occurring at lower elevations, reflecting the regional ice sheet surface gradient towards the retreating ice margin in the northwest. In the Kjølen mountains (Fig. 2), distinct meltwater channels occur from the highest elevation of ca. 1700 m a.s.l. (Tollan, 1963; Skjerven, 1978), and form a near-continuous series representing ca. 1000 m of ice sheet surface lowering, towards the valley floor of

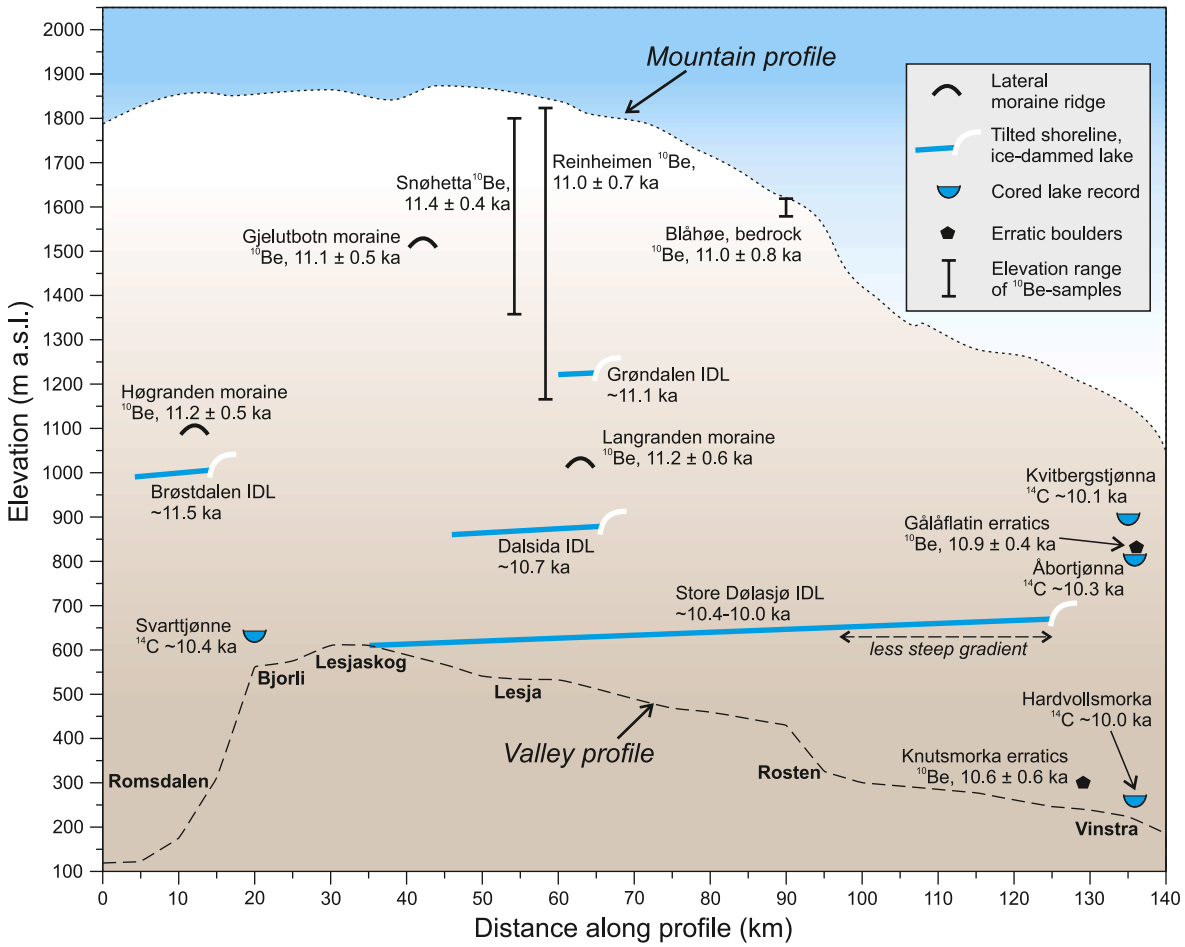

Fig. 11. NW-SE profile of the study area, summarizing all observations that have been used to reconstruct the development during Early Holocene ice-sheet thinning. All sample localities and obtained ages are plotted according to their position and elevation. The ages given for Reinheimen, Blåhøe and Snøhetta are arithmetic mean ages of 25, 11 and 15 samples, respectively.

Gudbrandsdalen. At ca. 1500 m a.s.l., a more than 2 km long, unbroken, and well-defined meltwater channel falls with a gradient near 20 m/km. Extended west, this gradient would correspond to ca. 900 m a.s.l. at the drainage divide at Lesjaskog (Fig. 12C and D), implying a reduction of ice thickness from ca. 1 km to 300 m over this distance, or even more due to a steeper ice surface gradient nearer the ice margin. In areas with well-developed meltwater channels, the elevation difference between individual channels is usually 5–20 m. Considering the calculated average ice sheet thinning rate from this study (1.7–5.8 m yr^{-1}), individual meltwater channels were generally active for a few years. However, in certain areas where lateral meltwater channels are closely located, they may also have formed and been active only during a single summer, as earlier suggested by Mannerfelt (1945).

The ice sheet eventually thinned to the saddle point between Gudbrandsdalen and Romsdalen, at Lesjaskog (610 m a.s.l., Fig. 2), which for several hundred years acted as a main spillway for meltwater from the rapidly decaying ice sheet in areas north of the ice divide of southern Norway. Lateral meltwater channels 2–5 km south of Svarttjønne, dip towards north with a gradient of ca. 25 m/km (Fig. 5). By extrapolating the gradient northwards, this corresponds to a level slightly below Svarttjønne, showing that the steep channels formed near the ice margin, and that ice remnants still occupied northern Gudbrandsdalen around 10.4 cal ka BP (Fig. 12D & E), when Svarttjønne and the drainage divide became ice free. During the following decay of the ice sheet, the Store Dølasjø formed (Fig. 12E & F). The investigated lakes Åbortjønna and Kvitbergstjønna are located on the mountain plateau (8–900 m a.s.l.), shortly south of the assumed position of the ice dam of the Store Dølasjø (Figs. 2 and 11), yet basal radiocarbon dates from these lakes pre-date the final drainage of the IDL. This suggests that the ice was less than 500 m thick and confined to the trunk valley of Gudbrandsdalen prior to the IDL drainage (Fig. 12E & F).

Several archaeological findings from the mountain region near the drainage divide, have been radiocarbon dated to the Early Holocene and overlap in time with the described deglaciation. Charcoal from a fireplace at 900 m a.s.l., located ca. 35 km north of Lesjaskog, was radiocarbon dated to ca. 10.8 cal ka BP (Fig. 12D; Breivik and Callanan, 2016), i.e., prior to deglaciation of the drainage divide at Lesjaskog and formation of the Store Dølasjø IDL. Another site at ca. 800 m a.s.l., near Romsdalen, has been dated to ca. 10.2 cal ka BP (Fig. 12E; M. Ramstad, pers. comm. 2023). The radiocarbon ages of charcoal are evidences for an ice-free landscape, as well as documenting that humans had started using this mountain region, probably for reindeer hunting (Breivik and Callanan, 2016; Glørstad, 2016). Glacier remnants, ice-dammed lakes and major glacial meltwater rivers were still present in the valleys and lowlands, and they likely determined the migration routes of reindeer as well as people. The deglaciation pattern constituted natural boundaries for the use of the landscape and its resources by early human inhabitants, well into the Holocene.

6. Conclusions

- The surface of the Scandinavian Ice Sheet remained well above 1800 m a.s.l. in the Gudbrandsdalen area throughout the Younger Dryas,

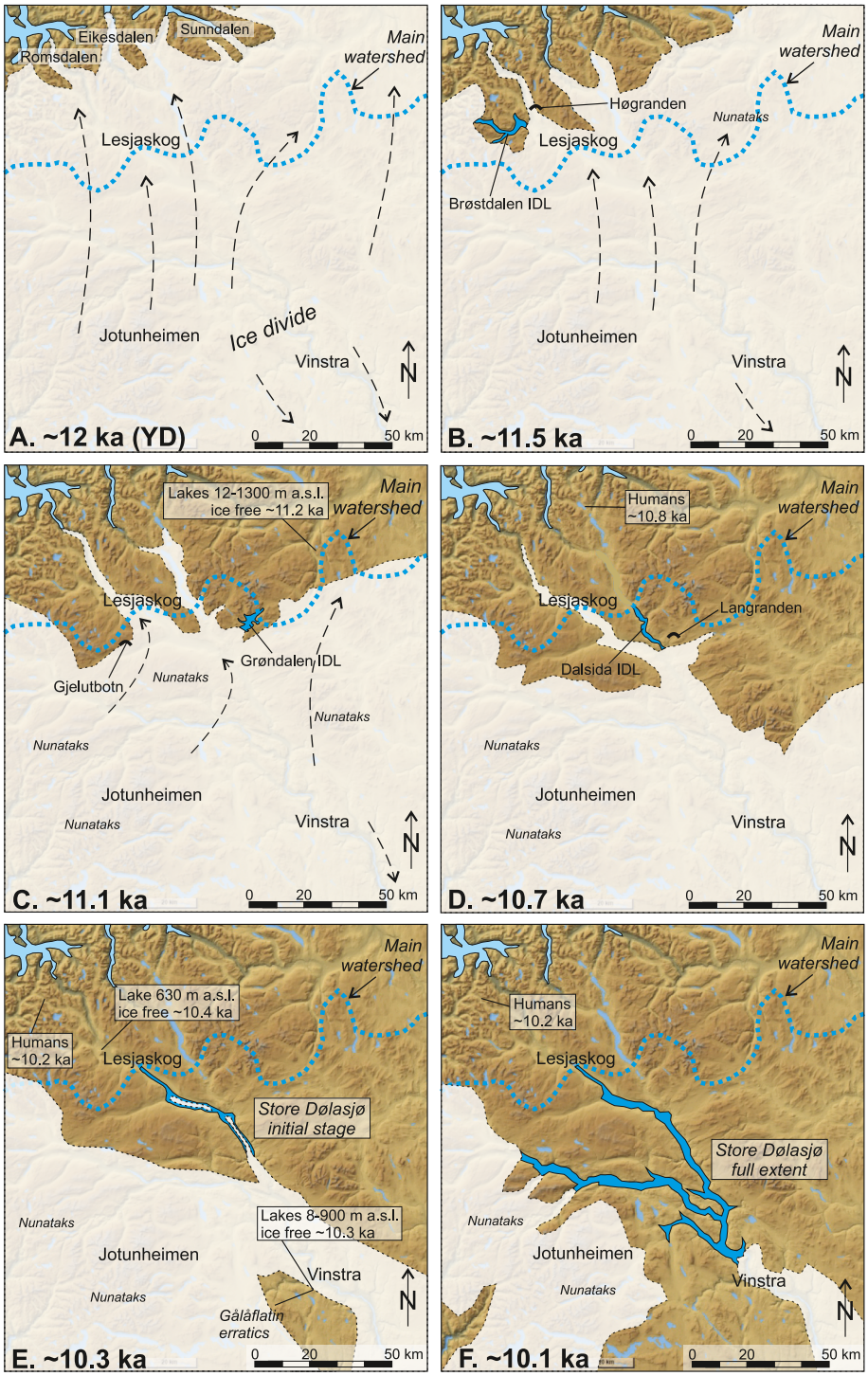

Fig. 12. Ice-sheet reconstructions for six selected time stages (A.-F.) during the final deglacation in northern Gudbrandsdalen. Note that nunatak areas were rapidly evolving during Early Holocene ice-sheet thinning; these are not precisely known and not shown on the maps. The palaeo-coastline is based on Svendsen and Mangerud (1987).

and most likely covered all adjacent mountains in central southern Norway.

- Following the Younger Dryas, the ice sheet thinned at average rates of 1.7–5.8 m yr^{-1} during the Early Holocene, and deglaciation was complete near 10.0 ka BP.
- The ice-sheet thinning estimate exceeds modelled thinning rates from the ICE-6G and ICE7-G models following the Younger Dryas by an order of magnitude.
- As the ice sheet thinned, various ice-dammed lakes formed between the ice sheet remnant and local drainage divides. Four major ice-dammed lakes have been mapped and their shoreline gradients show decreasing tilt with time and provide an independent chronology for the deglaciation.
- The largest ice-dammed lake, Store Dølasjø, developed after 10.4 ka BP and grew to a full extent of ca. 480 km^2 and a volume of about 80 km^3, before it drained at latest 10 ka BP.

Author contribution

Anders Romundset: Conceptualization, Methodology, Validation, Formal analysis, Investigation, Resources, Data curation, Writing – original draft, Visualization, Supervision, Project administration. Naki Akcar: Methodology, Formal analysis, Resources, Investigation, Writing – review & editing. Jane L. Andersen: Formal analysis, Visualization, Writing – review & editing. Ola Fredin: Methodology, Investigation, Visualization, Writing – review & editing. Fredrik Høgaas: Investigation, Writing – review & editing, Visualization. Marcus Christl: Resources. Serdar Yesilyurt: Formal analysis. Christian Schlüchter: Methodology, Investigation.

Declaration of competing interest

The authors declare that they have no known competing financial interests or personal relationships that could have appeared to influence the work reported in this paper.

Data availability

No data was used for the research described in the article.

Acknowledgements

The work was financed in collaboration by NGU and University of Bern. We thank the journal reviewers Anders Schomacker and anonymous for going carefully through our manuscript. Lina Gislefoss and Thomas Lakeman participated in the lake coring and Martin Klug helped with the scanning of sediment cores. Mikis van Boeckel produced the depth map and calculated the volume of the Store Dølasjø. Gaute Reitan, Morten Ramstad and Kristoffer Dahle aided with relevant archaeological literature. Jan Mangerud read the manuscript prior to submission and provided detailed criticism, comments, and ideas. We are most grateful for his enthusiastic and inspiring contribution, that greatly improved the final version of the paper.

Appendix A. Supplementary data

Supplementary data to this article can be found online at https://doi.org/10.1016/j.quascirev.2023.108274.

References

Aarseth, I., Austbo, P.K., Risnes, H., 1997. Seismic stratigraphy of Younger Dryas ice marginal deposits in western Norwegian fjords. Nor. Geol. Tidsskr. 77, 65–85.
Akçar, N., Deline, P., Ivy-Ochs, S., Alfimov, V., Hajdas, I., Kubik, P.W., Christl, M., Schlüchter, C., 2012. The AD 1717 rock avalanche deposits in the upper Ferret Valley (Italy): a dating approach with cosmogenic 10Be. J. Quat. Sci. 27, 383–392.
Andersen, B.G., Mangerud, J., Sørensen, R., Reite, A., Sveian, H., Thoresen, M., Bergstrøm, B., 1995. Younger-Dryas ice-marginal deposits in Norway. Quat. Int. 28, 147–169.
Andersen, J.L., Egholm, D.L., Knudsen, M.F., Linge, H., Jansen, J.D., Goodfellow, B.W., Pedersen, V.K., Tikhomirov, D., Olsen, J., Fredin, O., 2018. Pleistocene evolution of a Scandinavian plateau landscape. J. Geophys. Res.: Earth Surf. 123, 3370–3387.
Applegate, P.J., Urban, N.M., Keller, K., Lowell, T.V., Laabs, B.J., Kelly, M.A., Alley, R.B., 2012. Improved moraine age interpretations through explicit matching of geomorphic process models to cosmogenic nuclide measurements from single landforms. Quat. Res. 77, 293–304.
Balco, G., 2019. Isostatic rebound corrections are still on a squishy footing. Blog post retrieved from. https://cosmognosis.wordpress.com/2019/09/18/isostatic-rebound-corrections-are-still-on-a-squishy-footing/.
Balco, G., Stone, J.O., Lifton, N.A., Dunai, T.J., 2008. A complete and easily accessible means of calculating surface exposure ages or erosion rates from 10Be and 26Al measurements. Quat. Geochronol. 3, 174–195.
Bergersen, O.F., Garnes, K., 1971. Evidence of sub-till sediments from a weichselian interstadial in the Gudbrandsdalen valley, central east Norway. Norsk Geografisk Tidsskrift - Norwegian Journal of Geography 25, 98–107. https://doi.org/10.1080/00291957108551915.
Bergersen, O.F., Garnes, K., 1981. Weichselian in central south Norway: the gudbrandsdal interstadial and the following glaciation. Boreas 10, 315–322.
Bonow, J.M., Lidmar-Bergström, K., Näslund, J.-O., 2003. Palaeosurfaces and major valleys in the area of the Kjølen Mountains, southern Norway-consequences of uplift and climatic change. Norsk Geografisk Tidsskrift-Norwegian Journal of Geography 57, 83–101.
Borchers, B., Marrero, S., Balco, G., Caffee, M., Goehring, B., Lifton, N., Nishiizumi, K., Phillips, F., Schaefer, J., Stone, J., 2016. Geological calibration of spallation production rates in the CRONUS-Earth project. Quat. Geochronol. 31, 188–198.
Breivik, H.M., Callanan, M., 2016. Hunting high and low: postglacial colonization strategies in Central Norway between 9500 and 8000 cal BC. Eur. J. Archaeol. 19, 571–595.
Briner, J.P., Svendsen, J.I., Mangerud, J., Lohne, O.S., Young, N.E., 2014. A Be-10 chronology of south-western Scandinavian Ice Sheet history during the Lateglacial period. J. Quat. Sci. 29, 370–380. https://doi.org/10.1002/jqs.2710.
Bronk Ramsey, C., 2008. Deposition models for chronological records. Quat. Sci. Rev. 27, 42–60. https://doi.org/10.1016/j.quascirev.2007.01.019.
Bronk Ramsey, C., 2009. Bayesian analysis of radiocarbon dates. Radiocarbon 51, 337–360.
Chambers, R., 1851. 1. Personal observations on terraces, and other proofs of changes in the relative level of sea and land in scandinavia. Proceedings of the Royal Society of Edinburgh 2, 247–251.
Christl, M., Vockenhuber, C., Kubik, P.W., Wacker, L., Lachner, J., Alfimov, V., Synal, H.-A., 2013. The ETH Zurich AMS facilities: performance parameters and reference materials. Nucl. Instrum. Methods Phys. Res. Sect. B Beam Interact. Mater. Atoms 294, 29–38.
Dahl, S.O., Nesje, A., Øvstedal, J., 1997. Cirque glaciers as morphological evidence for a thin Younger Dryas ice sheet in east-central southern Norway. Boreas 26, 161–180.
Dortch, J.M., Tomkins, M.D., Saha, S., Murari, M.K., Schoenbohm, L.M., Curl, D., 2022. A tool for the ages: the probabilistic cosmogenic age analysis tool (P-caat). Quat. Geochronol. 71, 101323.
Follestad, B., Fredin, O., 2011. Geometry and vertical extent of the late Weichselian ice sheet in northwestern Oppland County, Norway. Norges Geologiske Undersøkelse Bulletin 451, 1–19.
Garnes, K., Bergersen, O.F., 1980. Wastage features of the inland ice sheet in central South Norway. Boreas 9, 251–269.
Gjessing, J., 1960. Isavsmeltningstidens drenening: dens forløp og formdannende virkning i nordre Atnedalen. Med sammenlignende studier fra nordre Gudbrandsdalen og nordre Østerdalen. Summary in English. Dr. Scient thesis, Universitetsforlaget.
Glørstad, H., 2016. Deglaciation, Sea-Level Change and the Holocene Colonization of Norway, vol. 411. Geological Society, London, Special Publications, pp. 9–25.
Goehring, B.M., Brook, E.J., Linge, H., Raisbeck, G.M., Yiou, F., 2008. Beryllium-10 exposure ages of erratic boulders in southern Norway and implications for the history of the Fennoscandian Ice Sheet. Quat. Sci. Rev. 27, 320–336.
Hansen, M.A., 1886. Om seter eller strandlinjer i store höjder over havet. Archiv Mathem. Naturv. 3, 329–352.
Hansen, A.M., 1890. Strandlinje-studier. Archiv Math. og Naturvidenskab 14, 254–343.
Heintz, A., 1955. The mammoth teeth from Norway. Norsk. Geogr. Tidsskr. b 34, 2–4.
Heintz, A., 1974. Two new finds and two new age-determinations of mammoths from Norway. Nor. Geol. Tidsskr. 54, 203–205.
Heyman, J., Stroeven, A.P., Harbor, J.M., Caffee, M.W., 2011. Too young or too old: evaluating cosmogenic exposure dating based on an analysis of compiled boulder exposure ages. Earth Planet Sci. Lett. 302, 71–80.
Høgaas, F., Longva, O., 2018. The late-glacial ice-dammed lake Nedre Glomsjø in Mid-Norway: an open lake system succeeding an actively retreating ice sheet. Norwegian Journal of Geology/Norsk Geologisk Forening 98.
Høgaas, F., Hansen, L., Berthling, I., Klug, M., Longva, O., Nannestad, H.D., Olsen, L., Romundset, A., 2023. Timing and Maximum Flood Level of the Early Holocene Glacial Lake Nedre Glomsjø Outburst Flood, Norway, Boreas.
Hole, J., Bergersen, O.F., 1981. Weichselian till stratigraphy and ice movements in Ottadalen, central south Norway. Norw. J. Geol. 61, 25–33.
Holmsen, G., 1916. Rendalens Bræsjö. In: NGU Aarbok, 79, pp. 1–37.
Holmsen, G., 1918a. Forskyvninger i snelinjens høide under avsmeltningsperioden. Nor. Geol. Tidsskr. 4, 63–84.
Holmsen, G., 1918b. Gudbrandsdalens bræsjø, Nor. Geol. Unders 83, 1–25.
Holmsen, G., 1965. Nyttbare Sand-Og Grusforekomster I Syd-Norge: De Geologiske Betingelser for Deres Avsetning, Universitetsforlaget.
Holtedahl, O., 1960. Geology of Norway. Norges geologiske undersøkelse 208, 1–540.
Hughes, A.L., Gyllencreutz, R., Lohne, Ø.S., Mangerud, J., Svendsen, J.I., 2016. The last Eurasian ice sheets–a chronological database and time-slice reconstruction, DATED-1. Boreas 45, 1–45.
Jones, R., Small, D., Cahill, N., Bentley, M., Whitehouse, P., 2019. iceTEA: tools for plotting and analysing cosmogenic-nuclide surface-exposure data from former ice margins. Quat. Geochronol. 51, 72–86.
Jowsey, P.C., 1966. An improved peat sampler. New Phytol. 65, 245–248.
Kubik, P.W., Christl, M., 2010. 10Be and 26Al measurements at the Zurich 6 MV Tandem AMS facility. Nucl. Instrum. Methods Phys. Res. Sect. B Beam Interact. Mater. Atoms 268, 880–883.
Lane, T., Paasche, Ø., Kvisvik, B., Adamson, K., Rodés, Á., Patton, H., Gomez, N., Gheorghiu, D., Bakke, J., Hubbard, A., 2020. Elevation changes of the Fennoscandian Ice Sheet interior during the last deglaciation. Geophys. Res. Lett. 47, e2020GL088796.
Lifton, N., Sato, T., Dunai, T.J., 2014. Scaling in situ cosmogenic nuclide production rates using analytical approximations to atmospheric cosmic-ray fluxes. Earth Planet Sci. Lett. 386, 149–160.

Linge, H., Brook, E.J., Nesje, A., Raisbeck, G.M., Yiou, F., Clark, H., 2006. In situ 10Be exposure ages from southeastern Norway: implications for the geometry of the Weichselian Scandinavian ice sheet. Quat. Sci. Rev. 25, 1097–1109.
Mangerud, J., 1963. Isavsmeltingen i og omkring midtre Gudbrandsdal. Nor. Geol. Unders 223, 223–274.
Mangerud, J., 1965. Dalfyllinger i noen sidedaler til Gudbrandsdalen, med bemerkninger om norske mammutfunn. Norsk geol. Tidsskr 50, 167–181.
Mangerud, J., Alexanderson, H., Birks, H.H., Paus, A., Perić, Z.M., Svendsen, J.I., 2023a. Did the Eurasian ice sheets melt completely in early Marine Isotope Stage 3? New evidence from Norway and a synthesis for Eurasia. Quat. Sci. Rev. 311, 108136.
Mangerud, J., Gyllencreutz, R., Lohne, Ø., Svendsen, J.I., 2011. Glacial history of Norway. In: Developments in Quaternary Sciences. Elsevier, pp. 279–298.
Mangerud, J., Goehring, B.M., Lohne, O.S., Svendsen, J.I., Gyllencreutz, R., 2013. Collapse of marine-based outlet glaciers from the scandinavian ice sheet. Quat. Sci. Rev. 67, 8–16. https://doi.org/10.1016/j.quascirev.2013.01.024.
Mangerud, J., Birks, H.H., Halvorsen, L.S., Hughes, A.L., Nashoug, O., Nystuen, J.P., Paus, A., Sørensen, R., Svendsen, J.-I., 2018. The timing of deglaciation and the sequence of pioneer vegetation at Ringsaker, eastern Norway–and an earthquake-triggered landslide. Nor. Geol. Tidsskr. 98, 301–318.
Mangerud, J., Hughes, A.L., Johnson, M.D., Lunkka, J.P., 2023b. The fennoscandian ice sheet during the younger Dryas stadial. In: European Glacial Landscapes. Elsevier, pp. 437–452.
Mannerfelt, C.M.s., 1945. Några glacialmorfologiska formelement: och deras vittnesbörd om inlandsisens avsmält-ningsmekanik I svensk och norsk fjällterräng. Geogr. Ann. 27, 3–5.
Mannerfelt, C.M.s., 1949. Marginal drainage channels as indicators of the gradients of Quaternary ice caps. Geogr. Ann. 31, 194–199.
Marr, P., Winkler, S., Binnie, S.A., Löffler, J., 2019. 10 Be-based exploration of the timing of deglaciation in two selected areas of southern Norway. E & G Quaternary Science Journal 68, 165–176.
Nesje, A., 1992. A piston corer for lacustrine and marine sediments. Arct. Alp. Res. 24, 257–259.
Nesje, A., Dahl, S.O., 1990. Autochthonous block fields in southern Norway: implications for the geometry, thickness, and isostatic loading of the Late Weichselian Scandinavian ice sheet. J. Quat. Sci. 5, 225–234.
Nesje, A., Anda, E., Rye, N., Lien, R., Hole, P.A., Blikra, L.H., 1987. The vertical extent of the Late Weichselian ice sheet in the Nordfjord-Møre area, western Norway. Nor. Geol. Tidsskr. 67, 125–141.
Nesje, A., Dahl, S.O., Anda, E., Rye, N., 1988. Block fields in southern Norway: significance for the Late Weichselian ice sheet. Nor. Geol. Tidsskr. 68, 149–169.
NGU, 2023. National Norwegian database of surficial deposits. Geol. Surv. Nor. 2023.
Noble, T., Rohling, E., Aitken, A., Bostock, H., Chase, Z., Gomez, N., Jong, L., King, M.A., Mackintosh, A., McCormack, F., 2020. The sensitivity of the Antarctic ice sheet to a changing climate: past, present, and future. Rev. Geophys. 58, e2019RG000663.
Øyen, P.A., 1896. Strandlinjer I Gudbrandsdalen, Af Peter Annaeus Øyen, A. Cammermeyer.
Patton, H., Hubbard, A., Andreassen, K., Auriac, A., Whitehouse, P.L., Stroeven, A.P., Shackleton, C., Winsborrow, M., Heyman, J., Hall, A.M., 2017. Deglaciation of the Eurasian ice sheet complex. Quat. Sci. Rev. 169, 148–172.
Paus, A., Velle, G., Berge, J., 2011. The Lateglacial and early Holocene vegetation and environment in the Dovre mountains, central Norway, as signalled in two Lateglacial nunatak lakes. Quat. Sci. Rev. 30, 1780–1796.
Paus, A., Boessenkool, S., Brochmann, C., Epp, L.S., Fabel, D., Haflidason, H., Linge, H., 2015. Lake Store Finnsjøen–a key for understanding Lateglacial/early Holocene vegetation and ice sheet dynamics in the central Scandes Mountains. Quat. Sci. Rev. 121, 36–51.
Peltier, W.R., Argus, D., Drummond, R., 2015. Space geodesy constrains ice age terminal deglaciation: the global ICE-6G_C (VM5a) model. J. Geophys. Res. Solid Earth 120, 450–487.
Pörtner, H.-O., Roberts, D.C., Adams, H., Adler, C., Aldunce, P., Ali, E., Begum, R.A., Betts, R., Kerr, R.B., Biesbroek, R., 2022. Climate Change 2022: Impacts, Adaptation and Vulnerability. IPCC Geneva, Switzerland.
Prud'Homme, C., Vassallo, R., Crouzet, C., Carcaillet, J., Mugnier, J.l., Cortés-Aranda, J., 2020. Paired 10Be sampling of polished bedrock and erratic boulders to improve dating of glacial landforms: an example from the Western Alps. Earth Surf. Process. Landforms 45, 1168–1180.
Regnéll, C., Mangerud, J., Svendsen, J.I., 2019. Tracing the last remnants of the Scandinavian Ice Sheet: ice-dammed lakes and a catastrophic outburst flood in northern Sweden. Quat. Sci. Rev. 221, 105862.
Reimer, P.J., Austin, W.E., Bard, E., Bayliss, A., Blackwell, P.G., Ramsey, C.B., Butzin, M., Cheng, H., Edwards, R.L., Friedrich, M., 2020. The IntCal20 Northern Hemisphere radiocarbon age calibration curve (0–55 cal kBP). Radiocarbon 62, 725–757.
Rekstad, J.B., 1896. Mærker efter istiden i det nordlige af Gudbrandsdalen. Archiv for Mathematik og Naturvidenskab 18, 22–pp.
Rekstad, J.B., 1898. Mærker efter istiden i Gudbrandsdalen. In: Archiv for Mathematik og Naturvidenskab, 20, p. 18.
Reusch, H., 1894. Har der existeret store, isdæmmede indsjøer paa østsiden af Langfjeldene. Norges Geologiske Undersøkelse 54, 51–59.
Reusch, H., 1910. De formodede strandlinjer i øvre Gudbrandsdalen. Norges Geologiske Undersøkelse 57 (24).
Romundset, A., Akçar, N., Fredin, O., Tikhomirov, D., Reber, R., Vockenhuber, C., Christl, M., Schlüchter, C., 2017. Lateglacial retreat chronology of the Scandinavian Ice Sheet in Finnmark, northern Norway, reconstructed from surface exposure dating of major end moraines. Quat. Sci. Rev. 177, 130–144. https://doi.org/10.1016/j.quascirev.2017.10.025.
Roy, K., Peltier, W.R., 2018. Relative sea level in the Western Mediterranean basin: a regional test of the ICE-7G_NA (VM7) model and a constraint on late Holocene Antarctic deglaciation. Quat. Sci. Rev. 183, 76–87.
Skjerven, J., 1978. Kvartærgeologiske Undersøkelser I Vågå-Området, Hovedoppgave I Kvartærgeologi Og Geomorfologi Ved Universitetet I Bergen.
Small, D., Bentley, M.J., Jones, R.S., Pittard, M.L., Whitehouse, P.L., 2019. Antarctic ice sheet palaeo-thinning rates from vertical transects of cosmogenic exposure ages. Quat. Sci. Rev. 206, 65–80.
Sollid, J., Kristiansen, K., 1984. Raumavassdraget, Kvartærgeologi Og Geomorfologi: 1: 80 000. Geografisk Institutt. Universitetet i Oslo.
Sollid, J.L., Sørbel, L., 1979. Deglaciation of western central Norway. Boreas 8, 233–239.
Sollid, J.L., Trollvik, J.A., 1991. Oppland Fylke, Kvartærgeologi Og Geomorfologi. Institutt for naturgeografi, Universitetet i Oslo.
Sørensen, R., Bakkelid, S., Torp, B., 1987. Land Uplift. Map Sheet 2.3.3., Norwegian Mapping Authority, *National Atlas of Norway. Main Topic 2: Landforms, Bedrock and Surficial Deposits*. Hønefoss.
Staiger, J., Gosse, J., Toracinta, R., Oglesby, B., Fastook, J., Johnson, J.V., 2007. Atmospheric scaling of cosmogenic nuclide production: climate effect. J. Geophys. Res. Solid Earth 112.
Stroeven, A.P., Heyman, J., Fabel, D., Björck, S., Caffee, M.W., Fredin, O., Harbor, J.M., 2015. A new Scandinavian reference 10Be production rate. Quat. Geochronol. 29, 104–115.
Stroeven, A.P., Hattestrand, C., Kleman, J., Heyman, J., Fabel, D., Fredin, O., Goodfellow, B.W., Harbor, J.M., Jansen, J.D., Olsen, L., Caffee, M.W., Fink, D., Lundqvist, J., Rosqvist, G.C., Stromberg, B., Jansson, K.N., 2016. Deglaciation of fennoscandia. Quat. Sci. Rev. 147, 91–121.
Svendsen, J.I., Mangerud, J., 1987. Late Weichselian and Holocene sea-level history for a cross-section of western Norway. J. Quat. Sci. 2, 113–132.
Svendsen, J.I., Briner, J.P., Mangerud, J., Young, N.E., 2015. Early break-up of the Norwegian channel ice stream during the last glacial maximum. Quat. Sci. Rev. 107, 231–242.
Tollan, A., 1963. Trekk av isbevegelsen og isavsmeltningen i Nordre Gudbrandsdalens fjelltrakter. Norges Geologiske Undersøkelse 223, 328–345.